RESEARCH MEMORANDUM

THEORETICAL DETERMINATION OF WATER LOADS ON PITCHING HULLS AND SHOCK-MOUNTED HYDRO-SKIS

By Emanuel Schnitzer

Langley Aeronautical Laboratory
Langley Field, Va.

NATIONAL ADVISORY COMMITTEE
FOR AERONAUTICS

WASHINGTON

October 19, 1956

NACA RM L56E31

NATIONAL ADVISORY COMMITTEE FOR AERONAUTICS

RESEARCH MEMORANDUM

THEORETICAL DETERMINATION OF WATER LOADS ON PITCHING HULLS AND SHOCK-MOUNTED HYDRO-SKIS

By Emanuel Schnitzer

SUMMARY

A quasi-steady theory is developed for the unsteady plane motion of seaplanes with high length-beam ratios and of shock-mounted hydro-skis impacting on a water surface while undergoing pitching rotation. This theory is based on a dynamic-camber equivalent in which a pitching flat plate immersed in a stream is replaced instantaneously by a stationary cambered airfoil for which similar fluid particle trajectories exist at the boundary. Since experimental hydrodynamic data were unavailable for verification of the proposed theory, comparisons are made with classical two- and three-dimensional linearized airfoil theory for steady and unsteady submerged motion and with a more approximate method that neglects the rotational effect on the pressure distribution. The agreement with the two-dimensional unsteady oscillating airfoil theory is not very good because of the presence of a large unsteady circulation term but the three-dimensional comparisons, which include, in addition, some oscillating airfoil data of aspect ratio 2, indicate fair agreement. The effect of rotation on the longitudinal pressure distribution for upward pitching is seen to broaden the stagnation peak and decrease the instantaneous ratio of maximum to average pressure, whereas downward pitching is seen to yield the opposite result. From the comparison with the more approximate method that neglects rotational effects on the pressure distribution, it is deduced that the effects of rotation might be important for some practical narrow-hull impacts but the more approximate theory could be used for the trimming shock-mounted hydro-ski cases considered. The loads predicted by the proposed theory for the trimming shock-mounted hydro-ski are less than those for the fixed-trim hydro-ski. The proposed theory might also be useful for calculations for a low-aspect-ratio pitching hydrofoil. Applications of a cambered airfoil theory to the determination of water-pressure distributions on hulls with pulled up bows are indicated. Appendixes containing exact solutions for the pressure distribution, load, and moment on a cambered airfoil immersed in a stream at a finite angle of attack are included. Step-by-step computational procedures with data-sheet headings for application of the proposed theory to seaplane hulls with high length-beam ratios and shock-mounted hydro-skis impacting on a water surface and involving rotation in pitch are also given in an appendix.

INTRODUCTION

This paper is concerned principally with the theoretical determination of the hydrodynamic loads and motions experienced by shock-mounted hydro-ski-equipped aircraft, seaplanes with high length-beam ratios, and other relatively narrow bodies undergoing unsteady planing motion on a water surface and involving pitching rotation. Although a water-impact theory for the freely trimming wide float has been developed, it is not believed that such a theory can be extended to cover the narrow-body case. Also, although much information is available for the oscillating airfoil covering a fairly complete range of aspect ratios from 0 to ∞, most of these theories are only applicable for small oscillations at small angles of attack. They are further restricted to deeply immersed bodies, whereas a hydro-ski or seaplane may have only the lower surface wetted. Another limitation to the use of the oscillating airfoil theory for unsteady planing on water arises because the wing-chord is constant, whereas the hydro-ski or flying-boat-hull wetted length is continually changing. Modifications of such airfoil theory to cover the hydrodynamic case have been made by Glauert and Perring (ref. 1) to take into account the surface of discontinuity and by Sedov (ref. 2) to include variable body shape and a changing wetted length.

In order to apply Sedov's method to nonharmonic motions such as water impacts, Fourier series solutions may be made. Such solutions are allowable since linearizing assumptions have been incorporated in the derivation. Since, however, hydro-skis operate at relatively high angles of attack, it is possible that such linearizations may not lead to reasonable approximations for actual operating conditions. This is one of the main reasons that these methods were not utilized in the present paper.

In order to obtain solutions to the unsteady planing problem applicable for practical angles of attack, an approximate dynamic-camber theory has been developed instead for the pressure distribution on pitching bodies during water impact. The purposes of this paper are to present this theory, to corroborate its accuracy insofar as possible, and to apply this theory and a more approximate version thereof to solving trimming hull and hydro-ski impact problems. The proposed dynamic-camber theory is based on the premise that a pitching flat plate deeply immersed in a stream may be replaced instantaneously by a stationary cambered airfoil for which similar flow particle trajectories exist at the boundary. It is believed allowable to apply this type of airfoil theory, where the entire foil is deeply immersed, to the hydrodynamic case where only the lower surface may be immersed in fluid, on the basis of Herbert Wagner's demonstration (ref. 3) that the longitudinal pressure distribution on the underside of a wing is very similar to that on the underside of a planing plate. The classical cambered airfoil theory is extended herein to include high angles of attack and finite cambers, which, when interpreted in terms of the pitching flat plate, are equivalent to appreciable

angular velocities at high trims. This equivalence comes from the quasi-steady adjustment of the airfoil camber at each instant to conform approximately to the instantaneous path lines of the particles moving along the rotating flat plate. Aspect-ratio corrections are applied to modify the pressure distributions for three-dimensional flow about the cambered airfoil.

In this paper an approximate theory for unsteady motion with rotation in pitch is first developed and compared with other theories and experimental data for oscillating wings. The load and motion equations for pitching hulls and hydro-skis are then developed and presented along with solutions for a few example cases. Several appendixes which are utilized in connection with the development of the theory and which present computational procedures for making solutions of pitching-hull and shock-mounted hydro-ski problems are included.

SYMBOLS

A	aerodynamic aspect ratio
B	ratio of average pressure in transverse plane to longitudinal center-line pressure in plane
b	beam of body
C_{cp}	center-of-pressure coefficient relative to step, $\frac{M_s}{F_N \lambda_w b}$
C_L	three-dimensional lift coefficient, $\frac{L}{\frac{\rho}{2} SU^2}$
c_l	section lift coefficient, $\frac{L/b}{\frac{\rho}{2} cU^2}$
C_m	three-dimensional moment coefficient, $\frac{M}{\frac{\rho}{2} ScU^2}$ or $\frac{M}{\frac{\rho}{2} \lambda_w^2 b^3 U^2}$
c_m	section moment coefficient, $\frac{M/b}{\frac{\rho}{2} c^2 U^2}$ or $\frac{M/b}{\frac{\rho}{2} \lambda_w^2 b^2 U^2}$
C_N	three-dimensional hydrodynamic-force coefficient, $\frac{F_N}{\frac{\rho}{2} \lambda_w b^2 U^2}$

[redacted]

c_N section hydrodynamic-force coefficient, $\frac{F_N/b}{\frac{\rho}{2}\lambda_w b U^2}$

C_Δ beam loading coefficient, $\frac{W}{\rho g b^3}$

c wing chord

D aerodynamic drag force, positive in aft direction

d damping exponent

E distance along ski between pivot and step or along hull between center of gravity and step measured parallel to keel, positive when measured aft (see fig. 5)

F force taken positive in upward or aft direction

f function

G damping constant, strut compression

G' damping constant, strut extension

g acceleration due to gravity

H coefficient in Blasius solution

h half height of cambered foil at maximum point (see fig. 2)

I pitching moment of inertia of trimming body

J distance between keel and center of gravity measured normal to keel (see fig. 5(a))

K spring force coefficient

k reduced-frequency parameter, $c\omega/2U$

$i = \sqrt{-1}$

L aerodynamic lift force, positive in upward direction

l length of body below undisturbed water surface (see fig. 5)

l_w length of body below elevated water surface (see fig. 5)

[redacted]

M	pitching moment, considered positive in a nose-up direction
P	distance along hydro-ski between pivot and shock-strut attachment
p	fluid pressure
q	resultant velocity of fluid, $\sqrt{u^2 + v^2}$
R	radius of cylindrical wing (see fig. 2)
r	longitudinal distance between step or trailing edge and center of pressure (see fig. 5)
$\mathcal{R}$	real part of
S	wing plan-form area
t	time
U	free-stream velocity at infinity for stationary body, and equivalent forward velocity $\dot{x} + \frac{\dot{z}}{\tan \tau} - z\dot{\tau}$ for moving body
u	velocity of fluid in X-direction
V	resultant velocity of impacting body
v	velocity of fluid in Y-direction
W	weight of aircraft supported by each hydro-ski or hull
w	complex potential
x_1	horizontal displacement for determination of equivalent camber
x	forward displacement of impacting body
y_1	vertical displacement for determination of equivalent camber
z	draft or downward displacement of body normal to undisturbed water surface
$Z = X + iY$ $Z' = X' + iY'$ $Z'' = X'' + iY''$	coordinate axes systems for conformal transformations (see fig. 2)

α inclination of stream flow to chord of airfoil (angle of attack)

Γ instantaneous circulation

γ flight-path angle

δ angle defining effective camber, $\frac{\dot{\tau}\lambda_w b}{2U}$ or $\frac{\dot{\alpha}c}{2U}$, radians

$\dot{\zeta}$ velocity of hull or hydro-ski normal to keel, positive downward

θ argument of Z''

κ approach parameter for free-body landing, $\frac{\sin \tau}{\sin \gamma_0}(\cos \tau + \gamma_0)$

λ length of float or hydro-ski below undisturbed water surface divided by mean beam

λ_w length of float or ski below elevated water surface divided by mean beam

ξ longitudinal distance along chord or keel measured from trailing edge, positive forward

ρ mass density of fluid

τ trim of ski or hull relative to undisturbed water surface, positive in nose-up direction

ϕ_L phase angle between angle-of-attack vector and lift vector, positive when angle-of-attack vector is leading

ϕ_M phase angle between angle-of-attack vector and moment vector, positive when angle-of-attack vector is leading

$\varphi(A)$ aspect-ratio correction

ω circular frequency of oscillation

Subscripts:

a at pivot (see fig. 5(b))

a' at connection point of shock strut to ski (see fig. 5(b))

e effective value

g gravity

[redacted]

LE	about leading edge
N	hydrodynamic normal
n	point number
0	at contact
p	aerodynamic pitching
r	hydrodynamic afterbody
s	about step
x	extrapolated quantity
α	derivative with respect to α
0,1,2,...	successive terms in a series
μ	about origin (located below midchord) (see Z-plane in fig. 2)
σ	maximum value
∞	infinity

A bar over a symbol means that the symbol pertains to the mass center of the trimming body or to the complex conjugate in appendixes A and B. An asterisk denotes that rotational effects have been included. Dots over symbols denote the derivatives with respect to time.

DEVELOPMENT OF THEORY FOR UNSTEADY MOTION WITH ROTATION IN PITCH

Concepts of Approach

In order to develop an approximate theory for the oblique impact or unsteady planing of a relatively narrow pitching body on a water-surface, the following reasoning was applied. First, for the simplified case of oblique impact at fixed trim, it has been shown in previous hydrodynamic publications that this case can be replaced at each instant by an equivalent planing case for which a similar load distribution exists. The criterion for this similarity was found to be that the horizontal velocity U of the forward intersection line of the body with the

water surface must be equal for both cases. This is demonstrated in the following sketches:

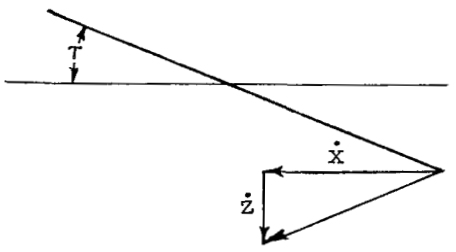

Fixed-trim impact

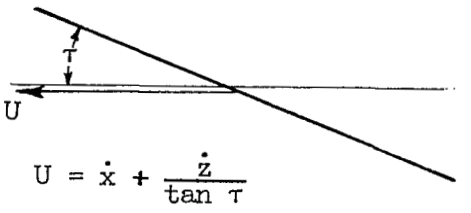

Equivalent planing

The effects of pitching rotation which are also taken into account in the present paper can be divided into two parts. The first part is the effect of the rotational velocity in modifying the effective planing velocity as illustrated by the following sketches:

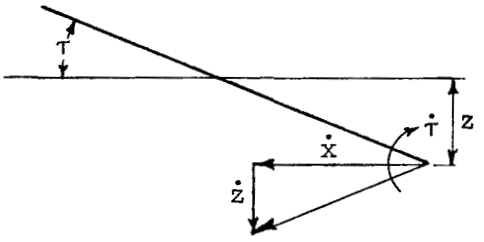

Trimming impact

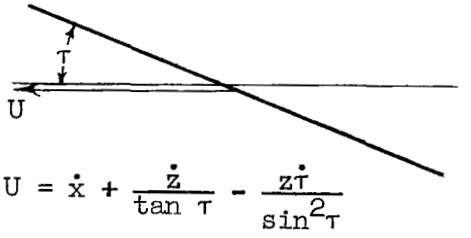

Equivalent planing (first approximating step)

The second part of the rotational effect is the modification of the longitudinal distribution of load or pressure caused by the influence of body rotation on the flow field. Although this second effect might be handled by classical oscillating airfoil theory, the two-dimensional theory does not apply for low-aspect-ratio bodies and the available low-aspect-ratio theory is not believed to give closed-form solutions. Therefore, a quasi-steady approximation was developed based on the premise that the effect of pitching rotation on a flat plate could be obtained from an instantaneously equivalent cambered airfoil planing on a water surface as shown

in the following sketches:

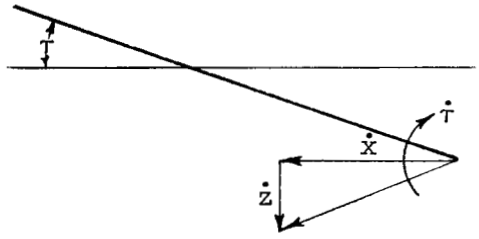

Trimming impact

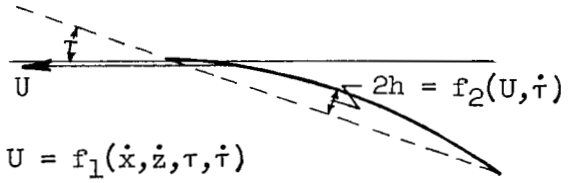

Equivalent planing (second approximating step)

The degree of camber $2h$ in the right-hand sketch, of course, depends on the pitching velocity.

The development and testing of this dynamic-camber concept is organized as follows. First, the cambered form is derived as the quasi-steady equivalent of the pitching wing. Then, the longitudinal pressure distribution is determined for the entire cambered form in deeply submerged flow and for a planing form with only the bottom side wetted. The application to water loads on pulled-up bows is indicated in passing. In order to verify the pressure distributions, loads and moments are obtained for the cambered form undergoing steady motion and are compared with linearized theory. The proposed dynamic-camber equations for the pitching wing are presented and tested at the zero-trim end point against classical two- and three-dimensional linearized airfoil theory for unsteady motion and with low-aspect-ratio oscillating airfoil data after incorporating the required aspect-ratio corrections into the proposed theory.

Derivation of Cambered Form as Quasi-Steady Equivalent of Pitching Wing

A simple quasi-steady theory for approximating the flow about a pitching two-dimensional flat-plate wing may be derived on the assumption that for relatively slow rotation the boundary for the pitching wing may be replaced at each instant by a different fixed-cambered boundary for which similar particle trajectories exist along the surface. Thus, the path lines traced by these particles during any small time interval would be similar for both cases. The fixed boundary is then defined by the motion of the particles during this small time interval along the flat surface of the plate which is rotating at some instantaneous angular velocity $\dot{\alpha}$ in a field of flow having a mean translational velocity U.

[redacted]

In order to determine the form of this fixed boundary, figure 1(a) which shows a sectional view of the rotating plate is introduced. From this figure the incremental horizontal distance traversed by a partical moving along the surface in the time dt is

$$dx_1 = U\,dt \tag{1}$$

In the same time interval the plate has rotated through the angle $d\alpha$. The approximate downwash velocities of the particle as it moves from the point x_1 to the point $x_1 + dx_1$ are given respectively by the equations

$$\left.\begin{aligned} \dot{y}_1 &= -U\alpha - x_1\dot{\alpha} \\ \dot{y}_1 + d\dot{y}_1 &= -U(\alpha + d\alpha) - (x_1 + dx_1)\dot{\alpha} \end{aligned}\right\} \tag{2}$$

The incremental change in downwash velocity expressed by $d\dot{y}_1$ should be identical to that for a particle moving along the hypothetical fixed-cambered boundary (fig. 1(b)) for which the downwash velocity at points x_1 and $x_1 + dx_1$ are, respectively, written

$$\left.\begin{aligned} \dot{y}_1 &= U\,\frac{dy_1}{dx_1} \\ \dot{y}_1 + d\dot{y}_1 &= U\left(\frac{dy_1}{dx_1} + d\,\frac{dy_1}{dx_1}\right) \end{aligned}\right\} \tag{3}$$

Therefore, equating the change in downwash $d\dot{y}_1$ for both the rotating plate and the stationary cambered plate and making use of equation (1) leads to the expression

$$d\dot{y}_1 = U\,d\,\frac{dy_1}{dx_1} = -2U\dot{\alpha}\,dt \tag{4}$$

Equation (4) can be integrated twice with respect to x_1, after again making use of equation (1), to yield the shape of the equivalent stationary cambered airfoil $y_1 = f(x_1)$ which is described by the equation

$$y_1 = -\alpha x_1 - \frac{\dot{\alpha}x_1^{\,2}}{U} \tag{5}$$

Equation (5) may be restated in nondimensional form by dividing by the half chord $c/2$

$$\frac{y_1}{c/2} = -\frac{x_1\alpha}{c/2} - \delta\left(\frac{x_1}{c/2}\right)^2 \tag{6}$$

where, for convenience, $\dot{\alpha}c/2U$ is designated δ. A plot of this equation is shown in figure 1(b) for $\alpha = 10^\circ$ and $\delta = 0.1$ which are believed to be realistic conditions for the trimming high-length-beam-ratio seaplane and for the shock-mounted trimming hydro-ski. If equation (6) is evaluated at the points $\frac{x_1}{c/2} = \pm 1$ (the leading and trailing edges of the cambered airfoil), it is found that

$$\left.\begin{aligned} \frac{y_1}{c/2} &= -\alpha - \delta \qquad \left(\frac{x_1}{c/2} = +1\right) \\ \frac{y_1}{c/2} &= \alpha - \delta \qquad \left(\frac{x_1}{c/2} = -1\right) \end{aligned}\right\} \tag{7}$$

so that in figure 1(b) the angles $\Delta\alpha = \pm\delta$ are seen to define the stationary cambered form. Therefore $\delta = \dot{\alpha}c/2U$ can be thought of as an effective instantaneous dynamic camber of a flat plate of chord c rotating at angular velocity $\dot{\alpha}$ in a stream flowing with velocity U.

Equation (6) is seen to represent a parabolic arc at an angle of attack α to the stream. It will be assumed for convenience that a circular arc will approximate equations (5) or (6) to a reasonable degree in this paper for application to calculations for practical hull or hydro-ski-equipped seaplanes. This is permitted since the maximum deviation between equation (6) and a circular arc drawn through the origin and end points of the example airfoil of figure 1(b) is of the order of 0.001c.

Longitudinal Pressure Distribution on Equivalent Circular-Arc Airfoil

In order to make solutions for the trimming plate it is first necessary to obtain the potential solution for the two-dimensional flow about the instantaneously equivalent circular-arc airfoil at finite angle of attack. This derivation is presented as appendix A and is an extension of the exact solution for a circular-arc airfoil at 0° angle of attack given in an appendix of reference 4. The solution presented herein is based on the transformation of the circle in the Z"-plane (see fig. 2) into the off-center circle in the Z'-plane which is then converted into

[redacted]

the circular-arc airfoil in the Z-plane by a Joukowski transform. The derivation was required since the pressure distribution on the lower surface of the plate must be known and it is not available from published thin airfoil theory. In addition, since large negative pressures are not believed to exist in the region of the forward water line, the concept of an effective length or chord c_e which extends from the rear of the airfoil forward to the point of zero pressure immediately ahead of the stagnation point will be applied. As stated in the introduction, justification for utilizing the lower surface pressure from the flow about a completely submerged body to represent the flow about a body planing on a surface of discontinuity was given by Wagner. This material is presented in figure 24 of reference 3 which presents a comparison of the immersed and planing cases up to relatively high trims. The agreement appears exceptional.

In figure 3 are presented plots of equations (A24) and (A26) of appendix A showing the variation, with fractional effective chord ξ/c_e of fluid pressure ratio $\frac{p}{\frac{1}{2}\rho U^2}$ on the lower surface of two-dimensional cambered plates. Here ξ is defined as the distance from the trailing edge measured forward along the chord and the pressure ratio is defined as the pressure at a point divided by the stagnation pressure due to the forward velocity. A wide range of trims and cambers are covered in these plots. Inspection of these pressure diagrams leads to the following two significant points on the behavior of a trimming hull or hydro-ski. Relative to the fixed-trim body, the effect of rotation which is a function of δ can be observed as a decrease in midchord pressure for downward trimming $(-\delta)$ which should shift the center of pressure forward, and an increase in midchord pressure for upward trimming (δ) which should shift the center of pressure aft. The effect of increasing angle of attack is to broaden the stagnation peak and decrease the instantaneous ratio of maximum pressure to average pressure while a decreasing angle of attack yields the opposite result. This effect may be significant for hulls having large bottom panels which might be designed stronger to withstand higher average pressures during upward pitching or having small bottom panels which might have to be stronger to take the high local pressures in downward pitching. The effects of rotation on pressure distribution may also be derived from classical linearized oscillating wing theory of reference 5.

Application of Pressure Distributions on Cambered Airfoils to Hulls or Hydro-skis Having Longitudinally Curved Bows

As stated previously, figure 3 presents longitudinal pressure distributions which may be directly applied in accordance with dynamic-camber

[redacted]

concepts to calculation of loads and motions of pitching hulls and hydro-skis with rectangular, flat bottoms. These pressure distributions may also be used directly for straight hulls and hydro-skis having curved-up bows during fixed-trim impact or planing on a water surface. In order to take into account the effect of aspect ratio for both of these cases however, a method which was devised in reference 6 is used. This method is described in detail in a subsequent section of this paper. When the plots of figure 3 are applied to bows of small upward curvature, the entire body may be considered to be curved longitudinally, the wetted chord extending from the step to the bow-water-air intersection. For large bow curvature, the body may be broken up into two lengths, straight and curved. The wetted chord of the bow arc extends from the forward edge of the straight section to the bow-water-air intersection. For this case, the overall longitudinal pressure distribution is made up of the pressure distribution for the curved section (δ finite) for the bow region and the distribution for the straight section wherein the whole body is assumed to be flat ($\delta = 0$). The forward part of the distribution for $\delta = 0$ extending over the curved-bow region is thrown away, the distribution for δ finite utilized in its place, and suitable fairing of the pressure curve at the body inflection point is employed. The normal-force coefficients required in applying the aspect-ratio correction may be determined from planing data obtained with the model in question or as a very rough approximation from the normal-force coefficients for the flat-plate case where the equivalent flat plate might possibly be represented by the wetted chord from the step to the bow-water-air intersection. The trim of this chord line is the trim used in obtaining theoretical or experimental normal-force coefficients for the flat-plate case.

Loads and Moments on Cambered Airfoil

In order to verify partially the theoretical pressure distributions for a cambered airfoil in deeply immersed flow as given in appendix A, the loads and moments obtained by integration of the pressure equations for small trims might be compared with classical linearized thin-airfoil theory. Direct integration of the proposed parametric pressure equations (A24) and (A26) in appendix A in order to obtain the loads and moments, however, appeared to be inconvenient so the method of Blasius (refs. 7 or 8) was used. Appendix B presents this solution.

The two-dimensional lift coefficient about the circular-arc airfoil for finite angles of attack is derived according to the method of Blasius in appendix B and is given as equation (B17). This equation is repeated here for convenience

$$c_l = \frac{L/b}{\frac{\rho}{2} cU^2} = 2\pi(\sin \alpha \cos \alpha + \cos^2\alpha \tan \delta) \qquad (8)$$

[redacted]

which, for small angles of attack and camber, reduces to the linearized equation for the thin airfoil (eq. 10.8, ch. II, ref. 9)

$$c_l = 2\pi\left(\alpha + 4\frac{h}{c}\right) \tag{9}$$

where $4\frac{h}{c} = \tan\delta$ is a measure of the camber as shown in figure 2 of the present paper. The upward trimming-moment coefficient about the leading edge for finite trims derived in appendix B as equation (B26) is

$$c_{m,LE} = \frac{M_{LE}/b}{\frac{\rho}{2}c^2U^2} = -\frac{\pi}{2}\left[\frac{\sin\alpha\cos\alpha}{\cos^2\delta} + \tan\delta(1 + \cos^2\alpha)\right] \tag{10}$$

which for small angles reduces to

$$c_{m,LE} = -\left(\frac{\pi}{2}\alpha + 4\pi\frac{h}{c}\right) \tag{11}$$

which is the same as the linearized equation for the thin airfoil (eq. 10.8, ch. II, ref. 9) except for the minus sign in equation (11) which arises from opposite positive moment conventions between this paper and reference 9.

Comparison of Dynamic-Camber Equations With Two- and Three-Dimensional Unsteady Linearized Airfoil Theory

It was shown previously that the angular velocity of an airfoil in plane motion involving pitching rotation could be expressed as an equivalent dynamic camber defined herein as $\delta = \dot{\alpha}c/2U$ where $\delta = \tan^{-1}4\frac{h}{c}$ for the equivalent stationary airfoil. If in equation (9) $4\frac{h}{c}$ is considered according to this dynamic-camber concept and $\dot{\alpha}c/2U$ is substituted in its place, then equation (9) can be considered as a linearized approximation to the two-dimensional rotational case for a flat plate. Since comparisons are to be made in this section with linearized theory where α approaches zero, the proposed theory will be altered similarly for this comparison with the result that $\tan\delta$ approaches δ. Equation (9) can therefore be rewritten as follows

$$c_l^* = 2\pi(\alpha + \delta) = 2\pi\left(\alpha + \frac{\dot{\alpha}c}{2U}\right) \tag{12}$$

[redacted]

where the asterisk denotes the added rotational effects. Rotation is assumed to occur about the center of the wing chord; hence, lift forces due to acceleration of the virtual mass are assumed to be nonexistent. The equation for the moment coefficient, on the other hand, should include a virtual mass torque which acts in the direction opposing the angular acceleration and has the form $-\frac{\pi c^2 \ddot{\alpha}}{64U^2}$. (See ref. 5.) Thus the equation for the two-dimensional moment coefficient about the origin including the effects of rotation may be written

$$c_{m\mu}^{*} = \frac{\pi\alpha}{2} - \frac{\pi c^2 \ddot{\alpha}}{64U^2} \tag{13}$$

In this equation the $\dot{\alpha}$ term drops out because of symmetry about the origin or midchord. This term appeared as the second term on the right side of equation (11) as $-4\pi\frac{h}{c}$.

A simple comparison between the linearized dynamic-camber equations (eqs. (12) and (13)) and the linearized theory for the oscillating airfoil (ref. 5) can be made for the case of a flat-plate airfoil at 0° angle of attack exhibiting small sinusoidal oscillations in attitude while immersed in a streaming fluid. For this case the instantaneous angle of attack may be expressed

$$\alpha = \alpha_\sigma e^{i\omega t} \tag{14}$$

where σ refers to the maximum value, i is the complex imaginary indicator $\sqrt{-1}$, ω is the circular frequency of oscillation, and t is the time. The instantaneous angular velocity and acceleration are therefore, respectively,

$$\dot{\alpha} = \frac{d\alpha}{dt} = i\omega\alpha_\sigma e^{i\omega t} = i\omega\alpha \tag{15}$$

$$\ddot{\alpha} = \frac{d^2\alpha}{dt^2} = -\omega^2\alpha_\sigma e^{i\omega t} = -\omega^2\alpha \tag{16}$$

Thus equation (12) may be restated as

$$\left.\begin{aligned} c_l^{*} &= 2\pi\left(\alpha + \frac{i\omega\alpha c}{2U}\right) \\ &= 2\pi\alpha_\sigma e^{i\omega t}\left(1 + \frac{i\omega c}{2U}\right) \end{aligned}\right\} \tag{17}$$

[redacted]

and, if $c\omega/2U$ is designated k, the reduced-frequency parameter of reference 5, this equation becomes

$$\frac{c_l^*}{\pi\alpha_\sigma} = 2\sqrt{1 + k^2}\, e^{i(\omega t + \tan^{-1} k)} \tag{18}$$

The comparable equation of Theodorsen (ref. 5) is

$$\frac{c_l^*}{\pi\alpha_\sigma} = \sqrt{(2F - kG)^2 + (k + kF + 2G)^2}\, e^{i\left(\omega t + \tan^{-1}\frac{k+kF+2G}{2F-kG}\right)} \tag{19}$$

for which the F and G functions have been evaluated and plotted in reference 5. (These functions are not defined in the present paper.) The amplitude of the lift vector of equation (18) is compared with that of equation (19) in figure 4(a) while the phase angles by which the lift leads the instantaneous angle of attack are compared in figure 4(b). In figure 4(a), considerable disagreement is shown between the proposed theory and that of reference 5 for calculating the magnitude of the lift vectors for the infinite-aspect-ratio case. Most of this discrepancy is believed to arise from the omission of certain frequency-sensitive circulation terms from equation (18) which are to be found in equation (19). The phase angles in figure 4(b) do not seem to be affected as severely.

The moment coefficient equation about the origin may be derived in a similar manner and is stated

$$\frac{c_{m\mu}^*}{\pi\alpha_\sigma} = \frac{1}{2}\left(1 + \frac{k^2}{8}\right)e^{i\omega t} \tag{20}$$

whereas the comparable Theodorsen equation is

$$\frac{c_{m\mu}^*}{\pi\alpha_\sigma} = \frac{1}{2}\sqrt{\left(\frac{kG}{2} - F - \frac{k^2}{8}\right)^2 + \left(\frac{k}{2} - G - \frac{kF}{2}\right)^2}\, e^{i\left(\omega t + \tan^{-1}\frac{\frac{k}{2} - G - \frac{kF}{2}}{\frac{kG}{2} - F - \frac{k^2}{8}}\right)} \tag{21}$$

where as before, the F and G functions are those which were tabulated in reference 5. The amplitude of the moment vector of equation (20) is compared with that of equation (21) in figure 4(c) and the phase angles by which the moment leads the instantaneous angle of attack are compared in figure 4(d). The disagreement between the moment vectors for the infinite-aspect-ratio case is similar in nature and magnitude with that of the lift vectors. The dynamic-camber system predicts no phase

[redacted]

difference between the moment vector and instantaneous angle of attack, whereas the exact theory shows a lagging phase angle. From these comparisons, it is concluded that the proposed theory should be used with caution for pitching bodies of large aspect ratio.

A better picture is presented for the case of low-aspect-ratio bodies which are the primary consideration in this paper. The dynamic-camber lift equation (12) may be further modified to include the effects of aspect ratio by assuming that both the term proportional to angle of attack and the term proportional to angular velocity of the airfoil are affected in a similar way by three-dimensional flow. On the basis of this assumption and utilizing Helmbold's airfoil aspect-ratio correction for zero sweep angle (refs. 10 and 11), equation (18) becomes

$$\frac{C_L^*}{\pi\alpha_\sigma} = 2\left(\frac{A}{2 + \sqrt{4 + A^2}}\right)\sqrt{1 + k^2}\, e^{i\left(\omega t + \tan^{-1}k\right)} \tag{22}$$

The aspect-ratio correction $\varphi(A) = \dfrac{A}{2 + \sqrt{4 + A^2}}$ is believed to be fairly accurate for all aspect ratios greater than 1. Equation (22) is plotted in figure 4(a) along with data obtained with an oscillating flat-plate airfoil of aspect ratio 2 (ref. 12). The three-dimensional linearized theory of reference 13 is also plotted for comparison. The agreement seems fair and probably indicates that the particular circulation term which was so affected by frequency for the infinite-span case is probably small for the low-aspect-ratio case. The phase-angle comparison, plotted in figure 4(b), also shows in general fair agreement for the low-aspect-ratio case.

As regards the pitching moment, the Helmbold aspect-ratio correction cannot generally be used since the shape of the longitudinal pressure distribution is believed to depend on aspect ratio. Therefore, for the moment case, aspect ratio is taken into account as follows: The two-dimensional dynamic-camber moment equation (13) may be extended to the three-dimensional case by assuming that the instantaneous longitudinal pressure distribution for the three-dimensional case is the same as that for the two-dimensional case having the same instantaneous section lift coefficient even though the trims are different for the two cases. This technique was applied to the nonrotating case in reference 6. On this basis, the linearized three-dimensional lift coefficient for fixed attitude may be expressed as

$$C_L = 2\pi\varphi(A)\alpha \tag{23}$$

[redacted]

where $\varphi(A)$ may be Helmbold's aspect-ratio correction for aspect ratios greater than 1. The desired two-dimensional section lift coefficient is obtained by dividing the actual three-dimensional lift coefficient by the ratio of the average pressure in a transverse plane to the pressure at the intersection of that plane with the longitudinal center line. Since reference 6 leaves this question open, a choice of Bobyleff's coefficient (refs. 14 and 15) has been made. Therefore, the desired section lift coefficient may be expressed as

$$c_l = \frac{2\pi\phi(A)\alpha}{B} = 2\pi\alpha_e \tag{24}$$

where $\alpha_e = \frac{\varphi(A)\alpha}{B}$ is the effective two-dimensional angle of attack giving the proper longitudinal center-line pressure distribution for the three-dimensional case of angle of attack α. The same aspect-ratio correction may be used for the $\ddot{\alpha}$ term as was used for the α term as long as the aspect ratio exceeds 1. For the hydro-ski case, smaller aspect ratios are encountered so that virtual mass terms might be modified for three dimensions by a more appropriate correction developed by Pabst (ref. 16) from measurements obtained on oscillating bodies submerged in water.

The moment coefficient about the midchord line for a trimming flat-plate airfoil having an aspect ratio greater than 1 is therefore obtained by applying the above technique to equation (13)

$$C_{m\mu}^* = \frac{B\pi\alpha_e}{2} - \frac{\pi c^2\ddot{\alpha}}{64U^2}\varphi(A)$$

$$= \left(\frac{\pi\alpha}{2} - \frac{\pi c^2\ddot{\alpha}}{64U^2}\right)\phi(A) \tag{25}$$

Since the term proportional to α does not appear in the dynamic-camber moment equation (eq. (13)) because of its symmetrical effect about the origin or moment axis, it is omitted here also. It is seen from equation (25) that, for the linearized case, the aspect-ratio correction may be applied to the section moment equation by direct multiplication as was done for the lift coefficient in equation (23). For sinusoidal oscillations, equation (25) becomes

$$\frac{C_{m\mu}^*}{\pi\alpha_\sigma} = \frac{\phi(A)}{2}\left(1 + \frac{k^2}{8}\right)e^{i\omega t} \tag{26}$$

[redacted]

This moment vector is plotted in figure 4(c) along with the data of reference 12 and the Lawrence and Gerber theory (ref. 13). The agreement also seems fair for the low-aspect-ratio case. The phase-angle data plotted in figure 4(d), however, predicts no phase lag for the dynamic-camber equations, whereas the more exact theory and the data do.

The above comparisons appear to substantiate use of the dynamic-camber concept for approximate calculation of forces and moments on low-aspect-ratio flat plates undergoing pitching rotation and translation while submerged in an infinite fluid. The extension of these concepts in the nonlinear form to the case of a pitching body planing on a surface of discontinuity is made on the basis of the previously mentioned similarity, demonstrated by Wagner, between the lower surface pressure distributions on the submerged airfoil and the planing plate. It is further believed that this concept may be extended to include other body shapes - for example, dead rise hulls and skis - after making suitable modifications to the design plots presented in a subsequent section of this paper.

LOAD AND MOTION EQUATIONS FOR BODIES UNDERGOING UNSTEADY PLANING WITH ROTATION IN PITCH

General Considerations

In order to determine the loads and motions of bodies undergoing combined rotation and translation through a water surface, the concept of an equivalent or effective planing velocity established in reference 17 is applied and extended to include rotational effects. This velocity U is derived with the aid of figure 5 from which it may be observed that the horizontal velocity of the keel-level water-intersection point relative to the step due to rotation is defined as

$$\text{Effective forward velocity} = -\frac{l\dot{\tau}}{\sin \tau} \tag{27}$$

The water rise is neglected in this calculation for simplicity since its effect is only noticed for short bodies as shown in reference 17 but it is included in computations of wetted area and aspect ratio as in reference 18. The effective forward velocity of an impacting body relative to the undisturbed water from translational motions is

$$\text{Effective forward velocity} = \dot{x} + \frac{\dot{z}}{\tan \tau} \tag{28}$$

The effective forward velocity of the keel-level water-intersection point is obtained through the summation in the horizontal direction of the

[redacted]

effective velocities derived from the rotational motion plus the effective velocities derived from the translational motions. Therefore, if equations (27) and (28) are combined with the equation $l = z/\sin\tau$, the effective planing velocity U of the keel-level water-intersection point with the step as a reference point is obtained as

$$U = \dot{x}_s + \frac{\dot{z}_s}{\tan\tau} - \frac{z_s\dot{\tau}}{\sin^2\tau} = \frac{\dot{\zeta} - l\dot{\tau}}{\sin\tau} \tag{29}$$

where $\dot{\zeta}$ is defined as the downward velocity of the hull or hydro-ski directed normal to the keel. The instantaneous velocity in combination with the instantaneous values of the dynamic camber δ, the trim τ, and the wetted length-beam ratio determine the load and load distribution on the impacting body including rotational effects.

The wetted-length—beam ratio λ_w is determined by the substitution into figure 6 of λ defined as the ratio of the length from step to keel-level water intersection to the beam. This plot is reproduced from reference 18 where it was constructed from the results of a planing-data analysis yielding the variation of the bow water rise for a rectangular flat plate.

The instantaneous two-dimensional hydrodynamic normal-force coefficient $c_N^* = \dfrac{F_N^*/b}{\frac{\rho}{2}\lambda_w b U^2}$ is obtained for each value of instantaneous trim and dynamic camber $\delta = \dfrac{\dot{\tau}\lambda_w b}{2U}$ by graphical integration of the lower-surface pressure distributions of figure 3. (The expression c_e in this figure is replaced by $\lambda_w b$ for the hydrodynamic case.) The resulting plot is presented as figure 7(a). The three-dimensional instantaneous hydrodynamic normal-force coefficient C_N^* is obtained through the use of the three-dimensional correction plotted in figure 8 which was derived from experimental high-speed planing data (ref. 19). For the endpoints of $\lambda_w = 0$ and $\lambda_w = \infty$, the theoretical solutions given in references 20 and 18, respectively, are plotted in figure 8 so that values of lift coefficient between the endpoints and the experimental length-beam ratios can be estimated. Since the same aspect-ratio correction is applied to the rotational component of the force as to the translational component as in equation (22), C_N^* may be substituted for C_N in the use of figure 8. Therefore, the c_N^* for any trim may be found on the $\lambda_w = 0$ curve and C_N^* is the value on the appropriate λ_w curve at the same trim. (Refer to line of long dashes in fig. 8.)

In order to determine the center-of-pressure coefficient about the step C^*_{cp} from which the instantaneous pitching moment is obtained, use is made of the effective trim concept mentioned in the previous section. This effective trim τ_e is obtained by substitution of the longitudinal-center-line normal-force coefficient $C_N{}^*/B$ into figure 8. The trim at which this value intersects the $\lambda_w = 0$ line is the effective two-dimensional trim. (Refer to line of short dashes in fig. 8.) This trim τ_e in combination with the value of δ previously selected may then be substituted into figure 7(b) to obtain the three-dimensional dynamic-camber center-of-pressure coefficient

$$C^*_{cp} = \frac{M_s{}^*}{F_N{}^* b \lambda_w} = \frac{C^*_{ms}}{C_N{}^*} \tag{30}$$

Figure 7(b) was also obtained from graphical integration of the pressure distributions of figure 3.

The effects of linear and angular acceleration of the virtual mass are neglected in this analysis since these terms are believed to be small for the quasi-steady, low-aspect-ratio case under consideration. The angular acceleration term is thought to be of the same order of magnitude as the term for the linear acceleration of the virtual mass normal to the keel, which was shown to be small for narrow bodies in reference 18.

Load and Motion Equations for Free-to-Trim Body Impacting on a Water Surface

The complete load and motion time histories for a freely trimming body impacting through a water surface may be determined by means of step-by-step methods of calculation. Since the instantaneous hydrodynamic force and moment may be computed approximately for any set of instantaneous conditions by means of the dynamic-camber analysis in the previous section entitled "General Considerations," it is necessary only to relate this force and moment to the dynamics of the body to obtain the incremental changes in accelerations, velocities, and drafts. The entire time histories can then be synthesized from these incremental steps.

The required load and motion equations may be set up with the aid of figure 5(a). The hydrodynamic force is assumed to be directed normal to the keel since viscous forces are usually small in hydrodynamic impact or high-speed planing. The force equation in the normal direction is therefore

$$\Sigma F = F_N + L - W \cos \tau = -\frac{W}{g} \ddot{\zeta} \tag{31}$$

[redacted]

If the aerodynamic lift L, which is taken normal to the keel, is assumed to be equal to the normal component of the weight, $L - W \cos \tau$ is equal to zero and these terms are eliminated from equation (31). The force equation for the direction parallel to the keel is omitted since for practical trims all forces in this direction are negligible.

The upward trimming moment about the center of gravity is

$$\Sigma \bar{M} = F_N(r - E) + \bar{M}_p + \bar{M}_r = \bar{I}\ddot{\tau} \tag{32}$$

Although the moment $\bar{M}_r$ arising from the hydrodynamic force on the afterbody is unknown at this writing, it is included to remind the reader that it is an extremely important term in many practical impacts and can only be neglected for portions of the impact where the moment contributed by the afterbody is negligible. If the aerodynamic lift is assumed to be colinear with the normal component of the weight force (aerodynamic moment equals zero), then $\bar{M}_p$ goes to zero and this term is eliminated from equation (32).

The effective forward velocity of the keel—level-water intersection in space may be obtained in a manner similar to that used in deriving equation (29) by vectorially adding the effective forward velocity due to translation of the center of gravity to the effective forward velocity due to rotation of the hull about the center of gravity. The resulting equation is

$$U = \frac{\dot{\bar{\zeta}} + (E - l)\dot{\tau}}{\sin \tau} \tag{33}$$

where $\dot{\bar{\zeta}}$ is obtained from integration of equation (31) and $\dot{\tau}$ from integration of equation (32).

The draft of the step z_s is obtained from the vector addition of the vertical displacement of the center of gravity and the vertical displacement of the step relative to the center of gravity and may be expressed as

$$z_s = \bar{z} + E(\sin \tau - \sin \tau_0) + J(\cos \tau - \cos \tau_0) \tag{34}$$

where the subscript 0 denotes the instant of contact between the water and the hull. A suggested step-by-step computational procedure for obtaining the load and motion time histories which utilizes the above equations is given in appendix C.

[redacted]

Load and Motion Equations for a Trimming Hydro-Ski Mounted on a Shock Strut and Impacting on a Water Surface

The trimming shock-mounted hydro-ski case is handled in a manner similar to that for the free-to-trim body. The equations of motion are derived with the aid of figure 5(b). The summation of forces on the hydro-ski normal to its keel, if the mass and inertia of the ski can be neglected, is

$$\Sigma F = F_N - F_a - F_{a'} = 0 \tag{35}$$

where the forces F_a and $F_{a'}$ are considered positive when they are acting upward on the fuselage. The summation of the forces on the fuselage normal to the hydro-ski keel is

$$\Sigma F = (L - W)\cos \tau + F_a + F_{a'} = -\frac{W}{g}\ddot{\zeta} = -\frac{W}{g}\ddot{\zeta}_a \tag{36}$$

where the assumption is made that the aircraft fuselage does not trim during the impact, and where F_a is the normal force applied at the pivot and $F_{a'}$ is the axial force applied by the shock strut which is assumed to be alined normal to the keel for convenience. The fixed-trim assumption has been borne out by experiments with hydro-ski equipped airplanes which showed little trim change of the fuselage during the immersed phase of any given impact.

The shock-strut reaction $F_{a'}$ for the general shock strut with the hydro-ski pivot in front as in figure 5(b) involving damping force proportional to some power of the telescoping velocity and some arbitrary form of springing is

$$F_{a'} = K\left[P(\tau_0 - \tau)\right] + G\left|P\dot{\tau}\right|^d \tag{37a}$$

for strut compression and

$$F_{a'} = -K\left[P(\tau - \tau_0)\right] - G'\left|P\dot{\tau}\right|^d \tag{37b}$$

for strut extension where K is the spring force function which, in general, may depend on $P(\tau - \tau_0)$ and in the linear spring case reduces to the ordinary spring constant, G and G' are the damping coefficients, and d is the damping exponent. For the case of the hydro-ski pivot behind the shock strut, G is replaced by $-G$ and $-G'$ is replaced by G'. The value of P is negative for this aft location of the hydro-ski pivot.

[redacted]

The upward trimming moment on the hydro-ski about the pivot (a) may be expressed as

$$\Sigma M_a = F_N(r - E) + F_a{}'P = I_a\ddot{\tau} = 0 \tag{38}$$

This sum is equal to zero since the inertia of the hydro-ski was assumed to be negligible. The moment on the fuselage must be equal to zero since the fuselage does not trim even though fuselage inertia is finite. The fuselage moment equation is not given here since it would serve no useful purpose in view of the fixed-trim qualification.

The effective forward velocity of the keel—level-water intersection in space given previously as equation (29) becomes in terms of the motions about the pivot point (a)

$$U = \dot{x}_a + \frac{\dot{z}_a}{\tan \tau} + \frac{(E - l)\dot{\tau}}{\sin \tau} \tag{39}$$

The draft of the step is determined by vector addition of the vertical displacement of the pivot and the vertical displacement of the step relative to the pivot and is expressed as

$$z_s = z_a + E(\sin \tau - \sin \tau_0) \tag{40}$$

The velocity of the point a (and the airplane) may be found from integration of equation (36) and the angular velocity and displacement may be obtained by integration of equation (38).

DISCUSSION OF SAMPLE SOLUTIONS

In order to demonstrate the application of the dynamic-camber theory to unsteady planing problems, several sample solutions have been made for chine-immersed impacts. These solutions have then been compared with further simplified theoretical solutions for which the effect of pitching rotation on the pressure distribution was ignored by setting $\delta = 0$ which for low trims is similar to the theory of reference 21. (When δ is set equal to zero for a pitching flat plate impacting through or planing on a water surface, the instantaneous pressure distribution on this plate is assumed in this paper to be the same as that for a similar plate steadily planing on a water surface at the same conditions of trim and draft at the forward velocity $\dot{x}$ which is equal to the effective forward velocity U of the body undergoing unsteady motion. Thus, the theory for $\delta = 0$ is termed herein as the effective forward velocity theory.) Comparisons were also made with still further simplified fixed-trim solutions ($\dot{\tau} = 0$) from reference 18 in order to demonstrate the effect on the hydrodynamic behavior of ignoring the trimming terms.

For simplicity, it has been assumed in the sample solutions that both hull forebody and ski bottoms are rectangular flat plates, that the aerodynamic lift is equal to, opposite, and colinear with the weight, and that the hull afterbody does not contact the water. A computation by the proposed methods for an actual impact does not have to be restricted to such a high degree if estimates of aerodynamic forces, afterbody water loads, and conversion factors for cross-sectional shapes other than the flat plate are available from theory or experiment.

Free-to-Trim Hull

Time-history solutions are presented in figures 9(a) and 9(b) for freely trimming, narrow hulls, restrained in yaw, roll, and lateral motions, impacting on a water surface. (See fig. 5(a).) The solutions for the vertical and trimming motions for a moderate beam loading $C_\Delta \approx 2$, where $C_\Delta = \frac{W}{\rho g b^3}$ are plotted in figure 9(a) with the contact conditions listed under run I in table I. For this case it is evident from figure 9(a) that the dynamic-camber solution does not differ greatly from the solution for $\delta = 0$ insofar as vertical acceleration of the aircraft is concerned but does give somewhat different rebound velocities ($\dot{z}$ at emergence from the water) and draft histories. The trimming velocity at rebound is also somewhat modified. Comparison with the fixed-trim theory indicates, as expected, large errors in trimming motion through use of the fixed-trim assumption but shows for this case that vertical accelerations of the center of gravity can be fairly closely estimated by the fixed-trim theory, whereas rebound velocity and draft history show some disagreement with trimming-theory results. Some of these results are more or less what would have been expected from a short extrapolation of the theoretical and experimental results for a nonchine-immersed, trimming float (ref. 22) into the moderately chine-immersed region. In this reference also, the effect of trimming in modifying the vertical center-of-gravity accelerations is shown to be small.

As the beam loading is increased so that deeper immersions with larger wetted-length-beam ratio λ_w result, the effect of rotation on the vertical motions was expected to increase for a given pitching moment of inertia since δ is proportional to λ_w. This is borne out in the solution for a higher beam loading $C_\Delta \approx 16$, presented in figure 9(b) with conditions at contact listed under run II in table I. For this case, figure 9(b) shows that the dynamic-camber solution departs still further from the solution for $\delta = 0$ although the difference in the maximum vertical acceleration of the center of gravity is not appreciable. The fixed-trim solution appears to give satisfactory results for this case only as a very crude approximation for the vertical motions after the

[redacted]

time of maximum acceleration. As a matter of interest, it might be pointed out that, in figures 9(a) and 9(b), the dynamic-camber solution falls between the fixed-trim solution and the solution for $\delta = 0$.

From figures 9(a) and 9(b) and the assumption that the dynamic-camber theory is valid at least for estimating rotational effects, it might be concluded that the proposed theory might be of some value in computing flying-boat landing characteristics for the following cases: where the shape of the load-time history is significant; where the trimming history is significant in determining the initial conditions of subsequent impacts; for seaplane porpoising calculations; or possibly for unsteady, low-aspect-ratio hydrofoil motions for both the deeply immersed case; and the case where the upper surface of the foil may be unwetted. The possibility should not be overlooked also that, for some flying-boat configurations, the effect of rotation on the vertical motions might be even more significant than that indicated in figures 9(a) and 9(b) since the sample cases chosen were selected more or less at random and are not necessarily typical of the worst cases. Also the effects of afterbody immersion and aerodynamic moments on the rotational velocity may increase the rotational effects on the pressure distribution. (Note that, for the sample cases of runs I and II, the rotational velocity at contact $\dot{\tau}_0$ is not very large.) A simple criterion for evaluation of the effects of rotation is the magnitude of δ which can be estimated for different hulls and impact or planing conditions.

Trimming Shock-Mounted Hydro-Ski

Time-history solutions are presented in figures 10(a) and 10(b) for water impacts of an aircraft equipped with pivoted hydro-skis with shock-strut restraint. (See fig. 5(b).) In these solutions, the following assumptions are made: the ski mass is negligibly small; the aircraft fuselage itself does not trim during the impact; the shock-strut spring force is proportional to the telescoping displacement; the damping force is proportional to the square of the telescoping velocity; and the shock-strut axis remains more or less normal to the hydro-ski keel.

The solution for a moderately high hydro-ski beam loading $(C_\Delta \approx 16)$ with the ski pivot forward of the shock strut is plotted in figure 10(a) with conditions at contact listed under run III in the table of initial conditions. The forward pivot location type of mounting is covered by the more general class of mountings for which the ski trim tends to decrease on contact with the water. The difference between the dynamic-camber solution and the solution for $\delta = 0$ for the case of figure 10(a) is seen to be practically insignificant. It probably would not be fair to compare the solutions for the trimming ski with those for the fixed-trim shock-mounted ski since the attachment point of the shock strut to the ski for the trimming case and the trim selected for the fixed-trim

case are believed to be critical. In order to make comparisons between these two types of mounting, some rational basis of comparison taking into consideration the effects of differences in the large number of existing independent variables must first be evolved. As a matter of interest, the fixed-trim solution (same case but with shock strut locked in extended position) is presented to indicate the degree of load alleviation obtainable for this example case with the shock-mounted trimming ski.

In figure 10(b) the solution for run IV in table I which involves a very high beam loading $\left(C_{\Delta} = 132\right)$ and a forward location of the ski pivot point is presented. For this case, the departure of the dynamic-camber solution from the solution for $\delta = 0$ is slightly greater than that for figure 10(a) as would be expected from an examination of the component values of δ. The heavier loading of the ski in run IV makes for larger λ_w which, as for the trimming hull, results in larger values of δ.

Apparently, from figures 10(a) and 10(b) for the trimming hydro-ski case with the forward pivot location, the theory for $\delta = 0$ may be substituted for the dynamic-camber theory for time-history calculations at least up to the time of maximum acceleration. Comparison in figure 10(b) with the fixed-trim solution (shock strut locked in the extended position) again shows the load reduction achieved with the trimming shock-mounted ski. For this case, the reduction in maximum load is considerably smaller than that for the lighter beam loading case of figure 10(a), whereas the ratio between the fixed and trimming times to peak load is greater for figure 10(b). For both cases, the rebound velocity is believed to be greatly reduced for the trimming mounting.

A further evaluation of the variation of the quantities making up δ indicated that, for those cases where the pivot is behind the shock strut or more generally where the ski trim increases on contact, the effect of trimming on the vertical motions might be greater. An attempt was made to make a numerical solution on an electronic digital computer for this case which was unsuccessful due to the choice of the number of significant figures used in the computer to describe the design charts in this paper. This part of the discussion is therefore included to caution the user of this type of computer to make use of an extra number of significant figures in the description of the design charts for cases with aft pivot locations. Although the preliminary work with the electronic digital computer indicated that the effect of rotation on the loads and motions was considerably increased for this case, further attempts were not made to obtain this solution since it was thought at this writing to be of less importance than runs III and IV. It is believed that numerical solutions for the case of the shock-mounted ski pivoted in the rear should not be exceptionally difficult where the right choices of increment size and number of significant figures are made.

[redacted]

CONCLUSIONS

The proposed dynamic-camber theory has been derived primarily for the analytical determination of the loads and motions of seaplanes with high length-beam ratios, shock-mounted hydro-skis and other bodies impacting or planing on a water surface while undergoing pitching rotation. Comparison of this theory with oscillating wing theory, with some low-aspect-ratio oscillating wing data, with a lower order unsteady planing approximation neglecting the effects of rotation on the pressure distribution (effective forward velocity theory), and with fixed-trim impact theory has led to the following conclusions:

1. The theoretical effect of rotational velocity on the longitudinal pressure distribution of a pitching flat plate for an increasing angle of attack is to broaden the stagnation peak and decrease the instantaneous ratio of maximum pressure to average pressure, whereas a decreasing angle of attack yields the opposite results. This effect is probably significant for hulls having large bottom panels which would have to be designed stronger to withstand high average pressures during upward pitching or small bottom panels which would have to be strong to take the high local pressures in downward pitching.

2. For the low-aspect-ratio case, the proposed theory, with the exception of the sensitive moment phase angle, is in fair agreement with Lawrence and Gerber's three-dimensional, unsteady, linearized airfoil theory and with some oscillating airfoil experiments for an aspect ratio of 2. For the infinite-aspect-ratio case, because of the lack of incorporation of a certain frequency-sensitive circulation term into the proposed theory, it is in relatively poor agreement with Theodorsen's exact, two-dimensional (infinite aspect ratio), unsteady, linearized airfoil theory for zero angle of attack. This circulation term is apparently unimportant for low aspect ratios.

3. For freely trimming, narrow seaplanes, the dynamic-camber, effective-forward-velocity, or fixed-trim theories give similar values of maximum acceleration but, where accurate time histories of translational and pitching motions are required, especially for the heavier beam loadings, a theory taking into account the effects of pitching rotation such as the dynamic-camber theory or some equivalent thereof is probably desired.

4. For trimming hydro-skis for which the trim decreases on contact (pivot located forward of the shock strut), both the dynamic-camber and effective-forward-velocity theories give similar results. Both theories predict load reductions for the trimming, shock-mounted hydro-ski over the equivalent fixed case (shock strut locked in the extended position) although for the higher beam loading, the load reduction was smaller for the cases examined, whereas the time to peak load was increased over the fixed trim case.

[redacted]

5. For low-aspect-ratio pitching hydrofoils either deeply immersed or planing on the surface, the dynamic-camber theory is believed to offer some promise.

Langley Aeronautical Laboratory,
National Advisory Committee for Aeronautics,
Langley Field, Va., May 24, 1956.

[redacted]

APPENDIX A

PRESSURE DISTRIBUTION ON A CAMBERED AIRFOIL AT LARGE ANGLES OF ATTACK

This appendix is concerned with the determination of the pressure distribution on a cambered airfoil at large angles of attack by means of conformal mapping procedures. This distribution is required for obtaining the loads and moments on such an airfoil.

The two-dimensional incompressible flow solution for a cambered airfoil at 0° angle of attack is given in appendix A of reference 4. Since the present paper is concerned with large angles of attack, a similar though more general analysis is required. This solution is developed with the aid of figure 2 as follows:

The exact complex potential for the flow including circulation about a circular cylinder of radius R for all angles of attack as represented by a section in the Z'' plane is (see ref. 8, arts. 6.22 and 7.12)

$$w = -U\left(Z''e^{-i\alpha} + \frac{R^2}{Z''e^{-i\alpha}}\right) - i\Gamma \log \frac{Z''}{R} \tag{A1}$$

where α is the angle of attack between the velocity vector U of the fluid far from the body and the negative X''-axis and Γ is a constant denoting the circulation.

The circle in the Z''-plane may be conformally transformed into a cambered airfoil in the Z-plane by first mapping it on the Z'-plane where it is converted to another circle of radius R the center of which is elevated in the Y'-direction a distance h. (See fig. 2.) The converting function required by this process is

$$Z'' = Z' - ih = Z' - \frac{ic}{4}\tan\delta \tag{A2}$$

where $c/4$ is the distance from the origin to the intercept of the circle on the X'-axis and $\tan\delta = 4\frac{h}{c}$. The circle on the Z'-plane is next converted to a circular-arc airfoil of length c and maximum ordinate $2h$ in the Z-plane by the Joukowski transformation

$$Z = Z' + \frac{(c/4)^2}{Z'} \tag{A3}$$

In order to determine the pressure distribution on this circular-arc airfoil, the velocity distribution about it must first be known. Before this velocity distribution can be determined, the circulation constant Γ of equation (A1) must first be determined with the aid of the Kutta condition, which predicts smooth flow at finite velocity off the trailing edge. Thus, the complex velocity dw/dZ must be finite at the point $Z = \frac{c}{2} + i0$ in the Z-plane which means that $dw/dZ' = 0$ at the point $Z' = \frac{c}{4} + i0$ in the Z'-plane. In other words, a stagnation point exists at the intercept of the circle and the positive X'-axis in the Z'-plane. Actually a stagnation point also exists at the point $Z' = -\frac{c}{4} + i0$ the intercept of the circle and the negative X'-axis.

The complex velocity about the circle in the Z'-plane may be obtained from the complex velocity in the Z"-plane by means of the following equation:

$$\frac{dw}{dZ'} = \frac{dw}{dZ''}\frac{dZ''}{dZ'} \tag{A4}$$

The complex velocity in the Z"-plane is obtained by taking the derivative of equation (A1) with respect to Z'' as follows:

$$\frac{dw}{dZ''} = -U\left(e^{-i\alpha} - \frac{R^2}{Z''^2 e^{-i\alpha}}\right) - \frac{i\Gamma}{Z''} \tag{A5}$$

Since $dZ''/dZ' = 1$, a combination of equations (A4) and (A5) yields the complex velocity in the Z'-plane which is

$$\frac{dw}{dZ'} = -U\left(e^{-i\alpha} - \frac{R^2}{Z''^2 e^{-i\alpha}}\right) - \frac{i\Gamma}{Z''} \tag{A6}$$

which is identical to equation (A5). In order to evaluate this expression at the trailing edge of the airfoil, the value of Z'' at the stagnation point $Z'' = \frac{c}{4} - \frac{ic}{4}\tan\delta = Re^{-i\delta}$ must be substituted into equation (A6) which then becomes

$$\frac{dw}{dZ'} = -U\left(e^{-i\alpha} - \frac{R^2}{R^2 e^{-2i\delta} e^{-i\alpha}}\right) - \frac{i\Gamma}{Re^{-i\delta}} \tag{A7}$$

[redacted]

Since the velocity at a stagnation point is equal to zero, equation (A7) is equated to zero and yields for the circulation constant

$$\Gamma = 2UR \sin(\alpha + \delta) \tag{A8}$$

If the circulation constant is inserted into equation (A6), the complex velocity in the Z'-plane becomes

$$\frac{dw}{dZ'} = -U\left[e^{-i\alpha} - \frac{R^2}{Z''^2 e^{-i\alpha}} + \frac{2iR \sin(\alpha + \delta)}{Z''}\right] \tag{A9}$$

The complex velocity in the Z-plane is obtained by means of the equation

$$\frac{dw}{dZ} = \frac{dw}{dZ'}\frac{dZ'}{dZ} = \frac{dw/dZ'}{dZ/dZ'} \tag{A10}$$

The expression for dZ/dZ' is obtained by differentiating the Joukowski transformation (eq. (A3)) with respect to Z' which yields

$$\frac{dZ}{dZ'} = 1 - \frac{(c/4)^2}{Z'^2} \tag{A11}$$

The general complex velocity of the fluid about the cambered wing in the Z-plane is obtained through combination of equations (A9), (A10), and (A11) and gives the equation

$$\frac{dw}{dZ} = \frac{-U\left[e^{-i\alpha} - \frac{R^2}{Z''^2 e^{-i\alpha}} + \frac{2iR \sin(\alpha + \delta)}{Z''}\right] Z'^2}{Z'^2 - \left(\frac{c}{4}\right)^2} \tag{A12}$$

The velocity at the surface of the airfoil may be determined through substitution of the expressions for Z'' and Z' on the body into equation (A12). These expressions in terms of the modulus and arguments of Z'' (R and θ, respectively) and the angle δ denoting the camber magnitude are

$$Z'' = Re^{i\theta} \tag{A13}$$

and

$$Z' = Re^{i\theta} + iR \sin\delta = R\left(e^{i\theta} + i \sin\delta\right) \tag{A14}$$

The complex velocity at the airfoil surface obtained through substitution of equations (A13) and (A14) and the expression $\frac{c}{4R} = \cos \delta$ into equation (A12) is written

$$\frac{dw}{dZ} = \frac{2iUe^{-i\theta}\left[\sin(\theta - \alpha) + \sin(\alpha + \delta)\right]\left(e^{i\theta} + i \sin \delta\right)^2}{\left(1 - 2ie^{i\theta}\sin \delta - e^{2i\theta}\right)} \tag{A15}$$

This complex fluid velocity may be subdivided into its components in the X- and Y-directions (u and v, respectively), by the equation

$$\frac{dw}{dZ} = -u + iv \tag{A16}$$

The square of the resultant velocity vector q is then obtained through multiplication of the complex velocity equation (A16) by its conjugate velocity $\left(\overline{\frac{dw}{dZ}}\right) = -u - iv$ as given by the equation

$$q^2 = u^2 + v^2 = \frac{dw}{dZ}\left(\overline{\frac{dw}{dZ}}\right) = \frac{dw}{dZ}\frac{d\overline{w}}{d\overline{Z}} \tag{A17}$$

This multiplication is easily accomplished through use of the following complex conjugate relations. If Q_1, Q_2, and Q_3 are three complex quantities and if

$$\frac{dw}{dZ} = Q_1Q_2Q_3 \tag{A18}$$

then

$$\left(\overline{\frac{dw}{dZ}}\right) = \overline{Q_1Q_2Q_3} = \overline{Q}_1\overline{Q}_2\overline{Q}_3 \tag{A19}$$

and therefore equation (A17) takes the form

$$q^2 = \frac{dw}{dZ}\left(\overline{\frac{dw}{dZ}}\right) = \left(Q_1\overline{Q}_1\right)\left(Q_2\overline{Q}_2\right)\left(Q_3\overline{Q}_3\right) \tag{A20}$$

Thus, q^2 may be obtained from equation (A15) by an operation similar to equation (A20) with the following result:

$$q^2 = \frac{\left(2iUe^{-i\theta}\right)\left(-2iUe^{i\theta}\right)\left[\sin(\theta - \alpha) + \sin(\alpha + \delta)\right]^2\left[\left(e^{i\theta} + i \sin \delta\right)\left(e^{-i\theta} - i \sin \delta\right)\right]^2}{\left(1 - 2ie^{i\theta}\sin \delta - e^{2i\theta}\right)\left(1 + 2ie^{-i\theta}\sin \delta - e^{-2i\theta}\right)}$$

[redacted]

or

$$q^2 = U^2\left[\frac{\cos\left(\alpha + \frac{\delta}{2} - \frac{\theta}{2}\right)}{\cos\left(\frac{\delta}{2} - \frac{\theta}{2}\right)}\right]^2 \left(1 + 2 \sin\theta \sin\delta + \sin^2\delta\right)^2 \tag{A21}$$

The distribution of the pressure p about the cambered airfoil may be determined by means of Bernoulli's equation which for the case of steady motion with viscous and gravitational forces neglected may be written as

$$p + \tfrac{1}{2}\rho q^2 = p_\infty + \tfrac{1}{2}\rho U^2 \tag{A22}$$

where p_∞ and U designate the pressure and velocity far away from the body. The pressure far from the body is set equal to zero; this condition allows equation (A22) to be written in nondimensional form as

$$\frac{p}{\frac{1}{2}\rho U^2} = 1 - \left(\frac{q}{U}\right)^2 \tag{A23}$$

The ratio of the pressure on the body to the stagnation pressure $\frac{1}{2}\rho U^2$ is then determined through combination of equations (A21) and (A23) and is written

$$\frac{p}{\frac{1}{2}\rho U^2} = 1 - \left[\frac{\cos\left(\alpha + \frac{\delta}{2} - \frac{\theta}{2}\right)}{\cos\left(\frac{\delta}{2} - \frac{\theta}{2}\right)}\left(1 + 2 \sin\theta \sin\delta + \sin^2\delta\right)\right]^2 \tag{A24}$$

It is noted that this pressure ratio appears as a function of the variable θ which is a parameter in this analysis since the position along the airfoil can also be obtained only as a function of θ. The X-location of the pressure is determined through combination of equations (A3), (A14), and the well-known relation $Re^{i\theta} = R(\cos\theta + i \sin\theta)$; thus,

$$Z = R\left\{\left[\cos\theta + i(\sin\theta + \sin\delta)\right] + \left(\frac{c}{4R}\right)^2\left[\frac{\cos\theta - i(\sin\theta + \sin\delta)}{\cos^2\theta + (\sin\theta + \sin\delta)^2}\right]\right\} \tag{A25}$$

and, since $\frac{c}{4} = R \cos \delta$, the real part of this expression becomes in dimensionless form

$$\frac{X}{c} = \frac{\cos \theta}{4 \cos \delta}\left(1 + \frac{\cos^2 \delta}{1 + 2 \sin \theta \sin \delta + \sin^2 \delta}\right) \tag{A26}$$

Thus, the pressure distribution about a two-dimensional cambered airfoil deeply immersed in a fluid and at any finite angle of attack is given by equations (A24) and (A26) where potential flow may be assumed.

[redacted]

APPENDIX B

LOADS AND MOMENTS ON A CAMBERED AIRFOIL OF INFINITE SPAN AT FINITE ANGLE OF ATTACK BY BLASIUS' THEORY

The loads and moments on a cambered airfoil might have been obtained through integration of the pressure distribution equations (A24) and (A26). It was believed to be simpler, however, to obtain these quantities by means of Blasius' theory (ref. 7, art. 7.1 or ref. 8, art. 6.4) by considering the flow far from the body.

According to Blasius, if the square of the complex velocity can be expressed by the series

$$\left(\frac{dw}{dZ}\right)^2 = H_0 + \frac{H_1}{Z} + \frac{H_2}{Z^2} + \cdots \tag{B1}$$

where H_0, H_1, H_2 . . . are independent of Z, then for large values of Z (far away from the body) the complex force on the body may be written as

$$\frac{D}{b} + \frac{iL}{b} = \pi\rho H_1 \tag{B2}$$

where D is the drag and L is the lift. The two-dimensional moment about the origin (located below the midchord in the Z-plane of fig. 2) M_μ/b may be written as:

$$\frac{M_\mu}{b} = \mathcal{R}(\pi\rho i H_2) \tag{B3}$$

where $\mathcal{R}$ refers to the real part of the expression.

In order to obtain dw/dz for the cambered wing in the appropriate form, equations (A2), (A3) (inverted), (A5), and (A8) are first restated as follows:

$$Z'' = Z' - ih$$

$$Z' = \frac{Z}{2} + \sqrt{\left(\frac{Z}{2}\right)^2 - \left(\frac{c}{4}\right)^2}$$

$$\frac{dw}{dZ''} = -U\left(e^{-i\alpha} - \frac{R^2 e^{i\alpha}}{Z''^2}\right) - \frac{i\Gamma}{Z''}$$

$$\Gamma = 2UR \sin(\alpha + \delta)$$

Equation (A2) transforms the symmetrically located circle in the Z"-plane into a displaced circle in the Z'-plane offset vertically upward a distance h. Equation (A3) is an inverted Joukowski transform which converts the offset circle in the Z'-plane to a circular arc of length c and maximum height $2h = \frac{c}{2} \tan \delta$ in the Z-plane. The positive sign for the radical was chosen since Z and Z' must both become large far from the body. Equation (A5) gives the general complex velocity of the fluid about the circle of radius R in the Z"-plane with circulation Γ where the resultant velocity of fluid U at ∞ is inclined at an angle α to the X"-axis.

The expression for the complex velocity in the Z-plane can be determined from the complex velocity in the Z"-plane by use of the relation

$$\frac{dw}{dZ} = \frac{dw}{dZ''} \frac{dZ''}{dZ} \tag{B4}$$

In order to obtain dZ''/dZ, Z" must first be expressed as a function of Z; this expression is obtained through a combination of equations (A2) and (A3) so that

$$Z'' = \frac{Z}{2} + \sqrt{\left(\frac{Z}{2}\right)^2 - \left(\frac{c}{4}\right)^2} - ih \tag{B5}$$

If the negative root had been chosen in equation (A3) instead of the positive one, then, as Z approaches ∞, Z" approaches 0 and this condition means that the flow outside the wing would be transformed to the inside of the circle instead of the outside of the circle for which the flow is defined. The derivative of Z" with respect to Z is therefore

$$\frac{dZ''}{dZ} = \frac{1}{2} + \frac{1}{2\sqrt{1 - \left(\frac{c}{2Z}\right)^2}} \tag{B6}$$

A combination of equations (A5), (B4), and (B6) results in the expression

$$\frac{dw}{dZ} = \left[\frac{1}{2} + \frac{1}{2\sqrt{1 - \left(\frac{c}{2Z}\right)^2}}\right]\left[-U\left(e^{-i\alpha} - \frac{R^2 e^{i\alpha}}{Z''^2}\right) - \frac{i\Gamma}{Z''}\right] \tag{B7}$$

[redacted]

In order to obtain the series expression for $(dw/dZ)^2$ required in equation (B1), the series for dw/dZ will be synthesized and then squared. The series for the first bracketed term from equation (754) of reference 23 may be written as

$$\frac{1}{2} + \frac{1}{2\sqrt{1 - \left(\frac{c}{2Z}\right)^2}} = 1 + \frac{\left(\frac{c}{4}\right)^2}{Z^2} + 3\frac{\left(\frac{c}{4}\right)^4}{Z^4} + 10\frac{\left(\frac{c}{4}\right)^6}{Z^6} + \cdots \tag{B8}$$

where $\left(\frac{c}{2Z}\right)^2$ approaches 0 for large values of Z far from the body, as required by Blasius' solution. The series for Z'' as a function of Z from equation (B5) and equation (753) of reference 23 may be written

$$Z'' = Z - ih - \frac{\left(\frac{c}{4}\right)^2}{Z} - \frac{\left(\frac{c}{4}\right)^4}{Z^3} - \frac{2\left(\frac{c}{4}\right)^6}{Z^5} - \cdots \tag{B9}$$

where $\left(\frac{c}{2Z}\right)^2$ approaches 0. The series for Z''^2 is therefore

$$Z''^2 = Z^2 - 2ihZ - \left[h^2 + 2\left(\frac{c}{4}\right)^2\right] + \frac{2ih\left(\frac{c}{4}\right)^2}{Z} - \frac{\left(\frac{c}{4}\right)^4}{Z^2} + \frac{2ih\left(\frac{c}{4}\right)^4}{Z^3} - \frac{2\left(\frac{c}{4}\right)^6}{Z^4} + \cdots \tag{B10}$$

The series expansion of dw/dZ may be synthesized from equations (B7), (B8), (B9), and (B10) and may be stated as

$$\frac{dw}{dZ} = \left[1 + \frac{\left(\frac{c}{4}\right)^2}{Z^2} + 3\frac{\left(\frac{c}{4}\right)^4}{Z^4} + \cdots\right]\left(-U\left\{e^{-i\alpha} - \frac{R^2 e^{i\alpha}}{Z^2 - 2ihZ - \left[h^2 + 2\left(\frac{c}{4}\right)^2\right] + \frac{2ih\left(\frac{c}{4}\right)^2}{Z} - \frac{\left(\frac{c}{4}\right)^4}{Z^2} + \cdots}\right\} - \frac{i\Gamma}{Z - ih - \frac{\left(\frac{c}{4}\right)^2}{Z} - \frac{\left(\frac{c}{4}\right)^4}{Z^3} - \cdots}\right) \tag{B11}$$

[redacted]

which, after multiplication and reduction, yields the equation for the first few terms which are all that are required in this paper

$$\frac{dw}{dZ} = -Ue^{-i\alpha} - \frac{i\Gamma}{Z} + \frac{1}{Z^2}\left[\Gamma h + UR^2e^{i\alpha} - U\left(\frac{c}{4}\right)^2 e^{-i\alpha}\right] + \ldots \tag{B12}$$

This expression is squared to again yield the first few terms required by the Blasius' solution for the square of the complex velocity

$$\left(\frac{dw}{dZ}\right)^2 = U^2e^{-2i\alpha} + \frac{2i\Gamma Ue^{-i\alpha}}{Z} - \frac{1}{Z^2}\left[\Gamma^2 + 2U\Gamma he^{-i\alpha} + 2U^2R^2 - 2U^2\left(\frac{c}{4}\right)^2 e^{-2i\alpha}\right] + \ldots \tag{B13}$$

Thus, the value for H_1 of equations (B1) and (B2) is from equations (A8) and (B13)

$$H_1 = 2i\Gamma Ue^{-i\alpha} = U^2ci\,\frac{\sin(\alpha + \delta)}{\cos\delta}(\cos\alpha - i\sin\alpha) \tag{B14}$$

since $R = \frac{c}{4}\cos\delta$. A combination of equations (B2) and (B14) yields the two-dimensional lift and drag forces

$$\frac{L}{b} = \pi\rho U^2c\,\frac{\cos\alpha}{\cos\delta}\sin(\alpha + \delta) \tag{B15}$$

$$\frac{D}{b} = \pi\rho U^2c\,\frac{\sin\alpha}{\cos\delta}\sin(\alpha + \delta) \tag{B16}$$

The section lift coefficient per unit span is therefore

$$c_l = \frac{L/b}{\frac{\rho}{2}(c)U^2} = 2\pi(\sin\alpha\cos\alpha + \cos^2\alpha\tan\delta) \tag{B17}$$

The moment is obtained in a similar manner. From equation (B13) the value of H_2 used in equations (B1) and (B3) is

$$H_2 = -\Gamma^2 - 2U\Gamma he^{-i\alpha} - 2U^2R^2 + 2U^2\left(\frac{c}{4}\right)^2 e^{-2i\alpha} \tag{B18}$$

The real part $\mathcal{R}$ of iH_2 is therefore

$$\mathcal{R}\,iH_2 = -2U^2\left(\frac{c}{4}\right)^2\sin 2\alpha + 2U\Gamma h\sin\alpha \tag{B19}$$

[redacted]

The two-dimensional pitching moment about the origin expressed positive for increasing α is therefore obtained from combining equations (A8), (B3), and (B19) with expressions $R = \frac{c}{4 \cos \delta}$ and $h = \frac{c}{4} \tan \delta$ to yield the equation

$$\frac{M_\mu}{b} = \frac{\pi \rho U^2 c^2}{4} \sin \alpha \cos \alpha (1 - \tan^2 \delta - \tan \alpha \tan \delta) \tag{B20}$$

The section moment coefficient per unit span about the origin is therefore

$$c_{M\mu} = \frac{M_\mu / b}{\frac{\rho}{2} c^2 U^2} = \frac{\pi}{2} \sin \alpha \cos \alpha (1 - \tan^2 \delta - \tan \alpha \tan \delta) \tag{B21}$$

In order to make comparisons with the thin airfoil low-angle derivation in chapter II of reference 9 (see eq. 10.8 of ref. 9), the moment must be taken about the leading edge. An upward pitching moment (increasing trim) is considered positive in this report and negative in reference 9 and thus have opposite signs. For small angles of attack, therefore, the two-dimensional upward trimming moment about the leading edge may be stated for the present derivation

$$\frac{M_{LE}}{b} = \frac{-L}{b}(c - r) = -\frac{L}{b}\left(\frac{c}{2} - r + \frac{c}{2}\right) \tag{B22}$$

where r is the distance between the center of pressure and the trailing edge. Since, however, the moment about the origin is

$$M_\mu = -L\left(\frac{c}{2} - r\right) \tag{B23}$$

the moment about the leading edge may be written

$$M_{LE} = -L \frac{c}{2} + M_\mu \tag{B24}$$

which, in combination with equations (B15) and (B20), becomes

$$\frac{M_{LE}}{b} = \frac{\pi \rho U^2 c^2}{4}\left[2 \frac{\cos \alpha}{\cos \delta} \sin(\alpha + \delta) - \sin \alpha \cos \alpha + \sin \alpha \cos \alpha \tan^2 \delta + \sin^2 \alpha \tan \delta\right] \tag{B25}$$

[redacted]

The upward trimming section moment coefficient per unit span about the leading edge is therefore

$$c_{m,LE} = \frac{M_{LE}/b}{\frac{\rho}{2}c^2U^2} = -\frac{\pi}{2}\left[\frac{\sin\alpha\cos\alpha}{\cos^2\delta} + \tan\delta\left(1 + \cos^2\alpha\right)\right] \qquad (B26)$$

[redacted]

APPENDIX C

METHODS OF SOLUTION

General.- The means for making numerical solutions of the equations for trimming bodies and shock-mounted hydro-skis are outlined in the following procedures. Step-by-step processes must be resorted to, because the equations do not lend themselves to explicit solution. Although the methods suggested depend on linear extrapolation, any well-known step-by-step procedures may be applied.

Both example procedures assume the immersing body to be a flat rectangular plate. In order to make solutions for other bottom shapes, the theory of references 6 and 18 or planing data obtained with the body of interest might be utilized in judicious modifications of the charts of figures 6 to 8 whereas a value of the coefficient B for average angles of dead rise greater than zero may be obtained from references 14, 15, or 18. The equations in this appendix include terms representing aerodynamic lift and pitching moment and hydrodynamic afterbody moment. In order to make fairly complete solutions by the proposed methods including the effects of these parameters on the overall hydrodynamic motions and loads, it is necessary to know the variations of the aerodynamic and afterbody terms with impact geometry either theoretically or from experimental data. Both solutions presented here assume that both aerodynamic and hydrodynamic forces are oriented essentially normal to the keel and neglect the force due to acceleration of the virtual water mass as was done in reference 18. The shock-mounted hydro-ski solution assumes that the mass and moment of inertia of the hydro-ski may be neglected, that exponential damping exists in the shock strut, and that the trim of the airplane is constant during impact. The water rise is taken into consideration only insofar as it affects the area over which the hydrodynamic force acts while the rate of change of water rise as a force increaser (see ref. 17) is neglected.

The numerical solutions are made with the aid of figures 5 to 8. Each time-history abscissa is subdivided into equal time increments of duration Δt where the subscript $n - 1$ designates the values calculated at the end of the previous time increment and n designates the values being calculated. For many applications it is believed to be advisable to select very small increments Δt for the first four or five steps and larger increments from there on. The correct increment size may be established by experience acquired in making several solutions for a given problem and using different increment sizes for each solution. The increment size may be increased until the point is reached where the solutions diverge from the more accurate curve obtained with a very small increment size. If a small-period oscillation is present in

the curve, too large an increment size or too small an increment size for the number of significant figures used to define the design curves is indicated. The first point in the time-history solution is determined by the initial conditions of the problem. The equations listed as computational steps outline the arrangement of computation sheets. The values determined from the repeated application of these equations when plotted against t give the motions of the trimming hull or the fuselage and shock-mounted hydro-ski as the case may be. For cases where δ is small, it may be taken as zero in order to simplify the calculations.

Computational steps for free-to-trim body with flat rectangular bottom.- The computational steps for a free-to-trim body with flat rectangular bottom are as follows:

(1) $$\tau_n = \tau_{n-1} + \dot{\tau}_{n-1}(\Delta t) + \frac{\ddot{\tau}_{n-1}(\Delta t)^2}{2}$$

(2) $$\dot{\bar{z}}_n = \dot{\bar{z}}_{n-1} + \ddot{\bar{\zeta}}_{n-1}(\Delta t)\cos \tau_{n-1}$$

(3) $$\bar{z}_n = \bar{z}_{n-1} + \frac{\dot{\bar{z}}_n + \dot{\bar{z}}_{n-1}}{2}(\Delta t)$$

(4) $$z_{sn} = z_{s(n-1)} + \bar{z}_n - \bar{z}_{n-1} + E(\sin \tau_n - \sin \tau_{n-1}) + J(\cos \tau_n - \cos \tau_{n-1})$$

(5) $$\lambda_n = \frac{z_{sn}}{b \sin \tau_n}$$

(6) $$\dot{\bar{\zeta}}_n = \dot{\bar{\zeta}}_{n-1} + \ddot{\bar{\zeta}}_{n-1}(\Delta t)$$

(7) $$\dot{\tau}_n = \dot{\tau}_{n-1} + \ddot{\tau}_{n-1}(\Delta t)$$

(8) $$U_n = \frac{\dot{\bar{\zeta}}_n + (E - \lambda_n b)\dot{\tau}_n}{\sin \tau_n}$$

(9) $$\lambda_{wn} = f(\lambda_n) \quad \text{(fig. 6)}$$

(10) $$\delta_n = \frac{\dot{\tau}_n \lambda_{wn} b}{2U_n} \quad \text{in radians}$$

$$\delta_n = \frac{28.65\dot{\tau}_n \lambda_{wn} b}{U_n} \quad \text{in degrees}$$

(11) $$c^*_{Nn} = f(\tau_n, \delta_n) \quad \text{(fig. 7(a))}$$

(12) $C^*_{Nn} = f\left(\lambda_{wn}, c^*_{Nn}\right)$ (See loop of long dashes in fig. 8)

(13) $F^*_{Nn} = C^*_{Nn} \frac{\rho}{2} \lambda_{wn} b^2 U_n^2$

(14) $\ddot{\zeta}_n = - \frac{F^*_{Nn} + (L_n - W)\cos \tau}{W/g}$

or, if wing lift may be assumed equal to the weight,

$$\ddot{\zeta}_n = - \frac{F^*_{Nn} g}{W}$$

(15) $\tau_{en} = f\left(\frac{C^*_{Nn}}{B}, \lambda_w = 0\right)$

where $B = 0.88$ (See loop of short dashes in fig. 8)

(16) $C^*_{cpn} = f(\tau_{en}, \delta_n)$ (fig. 7(b))

(17) $M^*_{sn} = F^*_{Nn} b \lambda_{wn} C^*_{cpn}$

(18) $\ddot{\tau}_n = \frac{M^*_{sn} - F^*_{Nn} E + \bar{M}_{pn} + \bar{M}_{rn}}{\bar{I}}$

or, if the resultant aerodynamic force may be assumed to pass through the center of gravity and to be equal to the weight,

$$\ddot{\tau}_n = \frac{M^*_{sn} - F^*_{Nn} E}{\bar{I}}$$

Computational steps for trimming rectangular flat-bottomed hydro-ski with shock-strut restraint.- The computational steps for trimming rectangular flat-bottomed hydro-ski with shock-strut restraint are as follows: (This method is for appreciable damping only. For cases of negligible damping on shock-strut extension (shock struts with dump valves), use this procedure until τ is a minimum, then use the following zero damping procedure until $z = 0$ again.)

(1) $\tau_n = \tau_{n-1} + \dot{\tau}_{n-1}(\Delta t) + \frac{\ddot{\tau}_{n-1}(\Delta t)^2}{2}$

(2) $\dot{z}_{an} = \dot{z}_{a(n-1)} + \ddot{\zeta}_{a(n-1)}(\Delta t)\cos \tau_{n-1}$

(3) $z_{an} = z_{s(n-1)} + \dot{z}_{a(n-1)}(\Delta t) + \frac{\ddot{\zeta}_{a(n-1)}\cos \tau_{n-1}(\Delta t)^2}{2} + E\left(\sin \tau_n - \sin \tau_{n-1}\right)$

(4) $\lambda_n = \dfrac{z_n}{b \sin \tau_n}$

(5) $\dot{\zeta}_{an} = \dot{\zeta}_{a(n-1)} + \ddot{\zeta}_{a(n-1)}(\Delta t)$

(6) $U_n = \dfrac{\dot{\zeta}_{an} + (E - \lambda_n b)\left(\dot{\tau}_{n-1} + \ddot{\tau}_{n-1}(\Delta t)\right)}{\sin \tau_n}$

(7) $\lambda_{wn} = f(\lambda_n)$ (fig. 6)

(8) $\delta_n = \dfrac{\lambda_{wn} b}{2U_n}\left(\tau_{n-1} + \ddot{\tau}_{n-1}(\Delta t)\right)$ (radians) $= \dfrac{28.65\lambda_{wn} b}{U_n}\left(\dot{\tau}_{n-1} + \ddot{\tau}_{n-1}(\Delta t)\right)$ (deg)

(9) $c^*_{Nn} = f(\tau_n, \delta_n)$ (fig. 7(a))

(10) $C^*_{Nn} = f\left(\lambda_w, c^*_{Nn}\right)$ (See loop of long dashes in fig. 8)

(11) $F^*_{Nn} = C^*_{Nn} \dfrac{\rho}{2} \lambda_{wn} b^2 U_n^2$

(12) $\ddot{\zeta}_{an} = -\dfrac{F^*_{Nn} + (L_n - W)\cos \tau_n}{W/g}$

or, if wing lift may be assumed equal to the normal component of the weight, then

$$\ddot{\zeta}_{an} = -\frac{F^*_{Nn} g}{W}$$

(13) $\tau_{en} = f\left(\dfrac{C^*_{Nn}}{B}, \lambda_{wn} = 0\right)$

where $B = 0.88$ (See loop of short dashes in fig. 8)

(14) $C^*_{cpn} = f(\tau_{en}, \delta_n)$ (fig. 7(b))

(15) $M^*_{sn} = F^*_{Nn} b \lambda_{wn} C^*_{cpn}$

[redacted]

$$(16)\quad \dot{\tau}_n = \pm \frac{1}{P}\left\{\frac{-M^*_{sn} + EF^*_{Nn} + PK\left[P(\tau_n - \tau_0)\right]}{GP}\right\}^{1/d}$$

where K in this case is a general spring function of $P(\tau_n - \tau_0)$, or for the special case of linear spring force (K = constant) and turbulent damping (d = 2)

$$\dot{\tau}_n = \pm\left[\frac{-M^*_{sn} + EF^*_{Nn} + KP^2(\tau_n - \tau_0)}{GP^3}\right]^{1/2}$$

where τ_n and τ_0 are expressed in radians. These equations apply only for strut compression where the hydro-ski pivot is in front of the shock strut. For extension of the strut with this arrangement the same equations apply with the exception that G is replaced by -G' which may have a different value. For the case of the hydro-ski pivot behind the shock strut, G is replaced by -G and -G' by +G'. Thus G changes sign when $\dot{\tau}$ goes through zero.

$$(17)\quad \ddot{\tau}_n = \frac{\dot{\tau}_n - \dot{\tau}_{n-1}}{(\Delta t)}$$

or more accurately to prevent divergence caused by small differences between $\dot{\tau}_n$ and $\dot{\tau}_{n-1}$

$$\ddot{\tau}_n = \frac{3\tau_n - 4\dot{\tau}_{n-1} + \dot{\tau}_{n-2}}{2(\Delta t)}$$

Computational steps for trimming rectangular flat plate hydro-ski with shock-strut restraint (zero damping).- The computational steps for trimming rectangular flat plate hydro-ski with shock-strut restraint (zero damping) are as follows:

(1) $\tau_x = \tau_{n-3} - 3\tau_{n-2} + 3\tau_{n-1}$

(Subscript x denotes extrapolation.)

(2) $\dot{z}_{an} = \dot{z}_{a(n-1)} + \ddot{\zeta}_{a(n-1)}(\Delta t)\cos\tau_{n-1}$

(3) $z_{sn} = z_{s(n-1)} + \dot{z}_{a(n-1)}(\Delta t) + \frac{\ddot{\zeta}_{a(n-1)}\cos\tau_{n-1}(\Delta t)^2}{2} + E(\sin\tau_x - \sin\tau_{n-1})$

(4) $\lambda_n = \frac{z_{sn}}{b\sin\tau_x}$

[redacted]

(5) $\dot{\zeta}_{an} = \dot{\zeta}_{a(n-1)} + \ddot{\zeta}_{a(n-1)}(\Delta t)$

(6) $U_n = \dfrac{\dot{\zeta}_{an} + (E - \lambda_n b)\left(\dot{\tau}_{n-1} + \ddot{\tau}_{n-1}(\Delta t)\right)}{\sin \tau_x}$

(7) $\lambda_{wn} = f(\lambda_n)$ (fig. 6)

(8) $\delta_n = \dfrac{\lambda_{wn} b}{2U_n}\left(\dot{\tau}_{n-1} + \ddot{\tau}_{n-1}(\Delta t)\right)$ in radians

$$\delta_n = \frac{28.65\lambda_{wn} b}{U_n}\left(\dot{\tau}_{n-1} + \ddot{\tau}_{n-1}(\Delta t)\right) \text{ in degrees}$$

(9) $c^*_{Nn} = f(\tau_x, \delta_n)$ (fig. 7(a))

(10) $C^*_{Nn} = f\left(\lambda_w, c^*_{Nn}\right)$ (See loop of long dashes in fig. 8)

(11) $F^*_{Nn} = C^*_{Nn} \dfrac{\rho}{2} \lambda_{wn} b^2 U_n^2$

(12) $\ddot{\zeta}_{an} = - \dfrac{F^*_{Nn} + (L_n - W)\cos \tau}{W/g}$

or if wing lift may be assumed equal to the normal component of the weight, then,

$$\ddot{\zeta}_{an} = - \frac{F^*_{Nn} g}{W}$$

(13) $\tau_{en} = f\left(\dfrac{C^*_{Nn}}{B}, \lambda_{wn}=0\right)$

where $B = 0.88$ (See loop of short dashes in fig. 8)

(14) $C^*_{cpn} = f(\tau_{en}, \delta_n)$ (fig. 7(b))

(15) $M^*_{sn} = F^*_{Nn} b \lambda_{wn} C^*_{cpn}$

[redacted]

$$(16)\quad \tau_n = \tau_0 + \frac{1}{P} K^{-1} \frac{M^*_{sn} - EF_{Nn}}{P}$$

for the general spring case where K^{-1} is the inverse spring function. For the special case of the linear spring (K = constant),

$$\tau_n = \tau_0 + \frac{M^*_{sn} - EF_{Nn}}{KP^2}$$

where τ_n and τ_0 are expressed in radians.

$$(17)\quad \dot{\tau}_n = \frac{\tau_n - \tau_{n-1}}{\Delta t}$$

$$(18)\quad \ddot{\tau}_n = \frac{\dot{\tau}_n - \dot{\tau}_{n-1}}{\Delta t}$$

[redacted]

REFERENCES

1. Perring, W. G. A., and Glauert, H.: The Stability on the Water of a Seaplane in the Planing Condition. R. & M. No. 1493, British A.R.C., 1933.

2. Sedov, L.: On the Theory of Unsteady Planing and the Motion of a Wing With Vortex Separation. NACA TM 942, 1940.

3. Wagner, Herbert: Planing of Watercraft. NACA TM 1139, 1948.

4. Kaplan, Carl: The Flow of a Compressible Fluid Past a Circular Arc Profile. NACA Rep. 794, 1944. (Supersedes NACA ARR I4G15.)

5. Theodorsen, Theodore: General Theory of Aerodynamic Instability and the Mechanism of Flutter. NACA Rep. 496, 1935.

6. Smiley, Robert F.: A Semiempirical Procedure for Computing the Water-Pressure Distribution on Flat and V-Bottom Prismatic Surfaces During Impact or Planing. NACA TN 2583, 1951.

7. Glauert, H.: The Elements of Aerofoil and Airscrew Theory. Second ed., Cambridge Univ. Press, 1947. (Reprinted 1948.)

8. Milne-Thomson, L. M.: Theoretical Hydrodynamics. The Macmillan Company, New York, 1950.

9. Von Kármán, Th., and Burgers, J. M.: General Aerodynamic Theory-Perfect Fluids. Theory of Airplane Wings of Infinite Span. Vol. II of Aerodynamic Theory, Div. E, ch. II, sec. 10, W. F. Durand, ed., Julius Springer (Berlin), 1935, pp. 48-53.

10. Helmbold, H. B.: Der unverwundene Ellipsenflügel als tragende Fläche. Jahrb. 1942 der Deutschen Luftfahrtforschung, R. Oldenbourg (Munich), pp. I-111 - I-113.

11. Polhamus, Edward C.: A Simple Method of Estimating the Subsonic Lift and Damping in Roll of Sweptback Wings. NACA TN 1862, 1949.

12. Widmayer, Edward, Jr., Clevenson, Sherman A., and Leadbetter, Sumner A.: Some Measurements of Aerodynamic Forces and Moments at Subsonic Speeds on a Rectangular Wing of Aspect Ratio 2 Oscillating About the Midchord. NACA RM L53F19, 1953.

13. Lawrence, H. R., and Gerber, E. H.: The Aerodynamic Forces on Low Aspect Ratio Wings Oscillating in an Incompressible Flow. Jour. Aero. Sci., vol. 19, no. 11, Nov. 1952, pp. 769-781. (Errata issued, vol. 20, no. 4, Apr. 1953, p. 196.)

[redacted]

14. Korvin-Kroukovsky, B. V., and Chabrow, Faye R.: The Discontinuous Fluid Flow Past an Immersed Wedge. Preprint No. 169, S.M.F. Fund Paper, Inst. Aero. Sci. (Rep. No. 334, Project No. NR 062-012, Office of Naval Res., Exp. Towing Tank, Stevens Inst. Tech.), Oct. 1948.

15. Lamb, Horace: Hydrodynamics. Sixth ed., Cambridge Univ. Press, 1932, pp. 94-105.

16. Pabst, Wilhelm: Landing Impact of Seaplanes. NACA TM 624, 1931.

17. Smiley, Robert F.: An Experimental Study of Water-Pressure Distributions During Landings and Planing of a Heavily Loaded Rectangular Flat-Plate Model. NACA TN 2453, 1951.

18. Schnitzer, Emanuel: Theory and Procedure for Determining Loads and Motions in Chine-Immersed Hydrodynamic Impacts of Prismatic Bodies. NACA Rep. 1152, 1953. (Supersedes NACA TN 2813.)

19. Weinstein, Irving, and Kapryan, Walter J.: The High-Speed Planing Characteristics of a Rectangular Flat Plate Over a Wide Range of Trim and Wetted Length. NACA TN 2981, 1953.

20. Pierson, John D., and Leshnover, Samuel: An Analysis of the Fluid Flow in the Spray Root and Wake Regions of Flat Planing Surfaces. Preprint No. 166, S.M.F. Fund Paper, Inst. Aero. Sci. (Rep. No. 335, Project No. NR 062-012, Office of Naval Res., Exp. Towing Tank, Stevens Inst. Tech.), Oct. 1948.

21. Froscher, Clarence T., and Greenwood, Robert B.: Analytical Determination of Lower Limit Stability of Flying Boats. Experimental Towing Tank, Stevens Inst. of Tech., May 1951.

22. Miller, Robert W.: Theoretical Analysis of Hydrodynamic Impact of a Prismatic Float Having Freedom in Trim. NACA TN 2698, 1952.

23. Pierce, B. O.: A Short Table of Integrals. Third rev. ed., Ginn & Co., 1929.

[redacted]

TABLE I.- INITIAL CONDITIONS OF IMPACT

Configuration	Trimming hull		Shock-mounted trimming ski	
Run	I	II	III	IV
b, ft	10	5	2	1
B	0.88	0.88	0.88	0.88
C_Δ	1.98	15.9	16.26	132
d	---	---	2	2
P, ft	---	---	10	10
E, ft	5	5	15	15
G, $\frac{\text{lb}}{\text{ft/sec}^2}$	---	---	412	412
$\bar{I}$, slug-ft^2	1,600,000	1,600,000	-----	-----
J, ft	14.7	14.7	-----	-----
K, lb/ft	---	---	7,500	7,500
U_o, ft/sec	---	---	223.5	223.5
$\bar{V}_o$, ft/sec	135	135	-----	-----
W, lb	123,500	123,500	8,250	8,250
z_o, ft	---	---	0	0
$\bar{z}_o$, ft	0	0	-----	-----
$\dot{z}_{a_o}$, ft/sec	---	---	17	17
$\dot{\bar{z}}_o$, ft/sec	22.2	22.2	-----	-----
β, deg	0	0	0	0
γ_o, deg	9.48	9.48	6.06	6.06
$\dot{\zeta}_{a_o}$, ft/sec	---	---	57.9	57.9
$\dot{\bar{\zeta}}_o$, ft/sec	34.9	34.9	-----	-----
$\ddot{\bar{\zeta}}_o$, ft/sec^2	0	0	-----	-----
$\ddot{\zeta}_{a_o}$, ft/sec^2	---	---	0	0
κ	0.592	0.592	2.23	2.23
ρ, slug-ft^3	1.938	1.938	1.938	1.938
τ_o, deg	5.5	5.5	15	15
$\dot{\tau}_o$, radian/sec	-0.087	-0.087	0	0
$\ddot{\tau}_o$, radian/sec^2	0	0	0	0

[redacted]

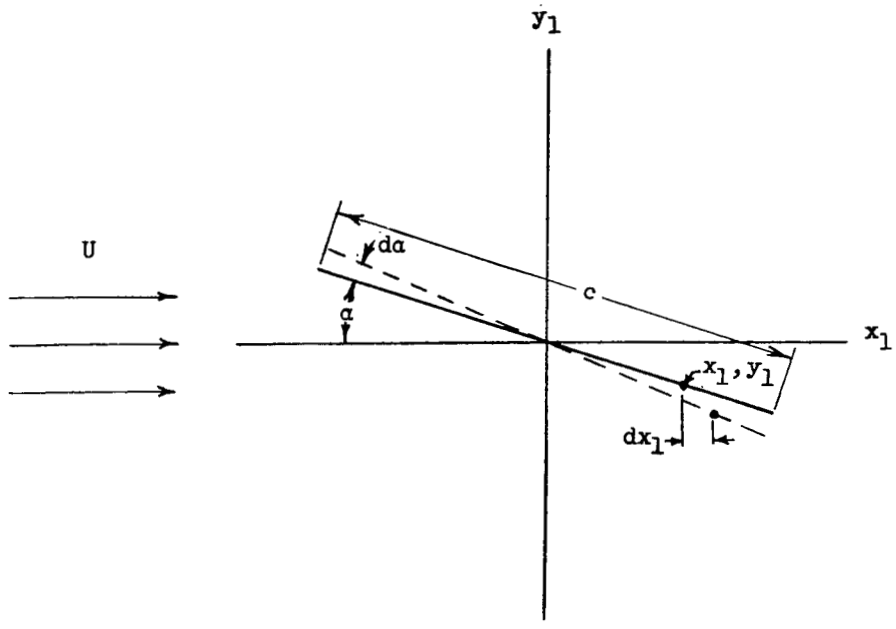

(a) Rotating plate in stream.

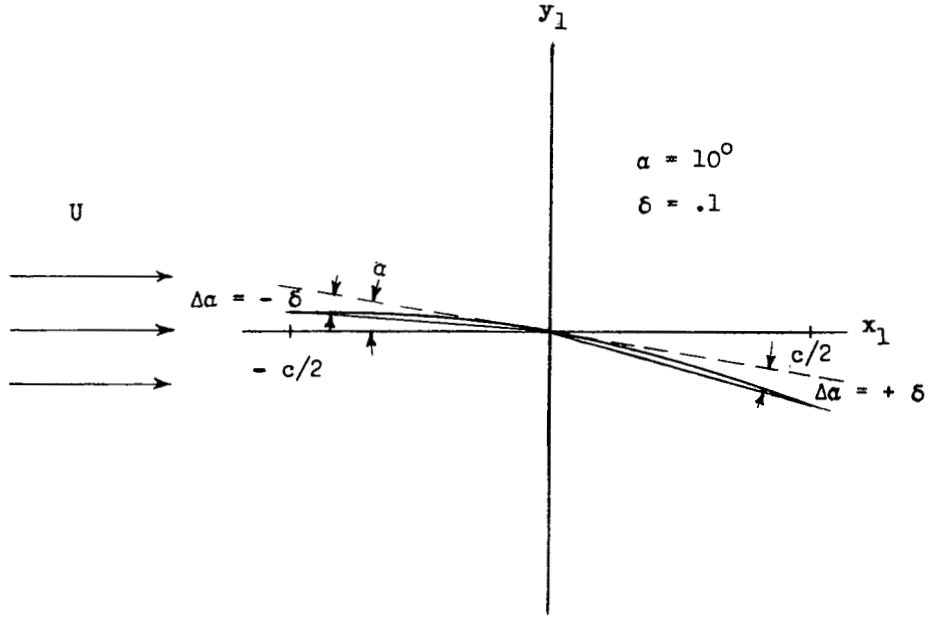

(b) Equivalent cambered plate in stream.

Figure 1.- Shape of cambered boundary.

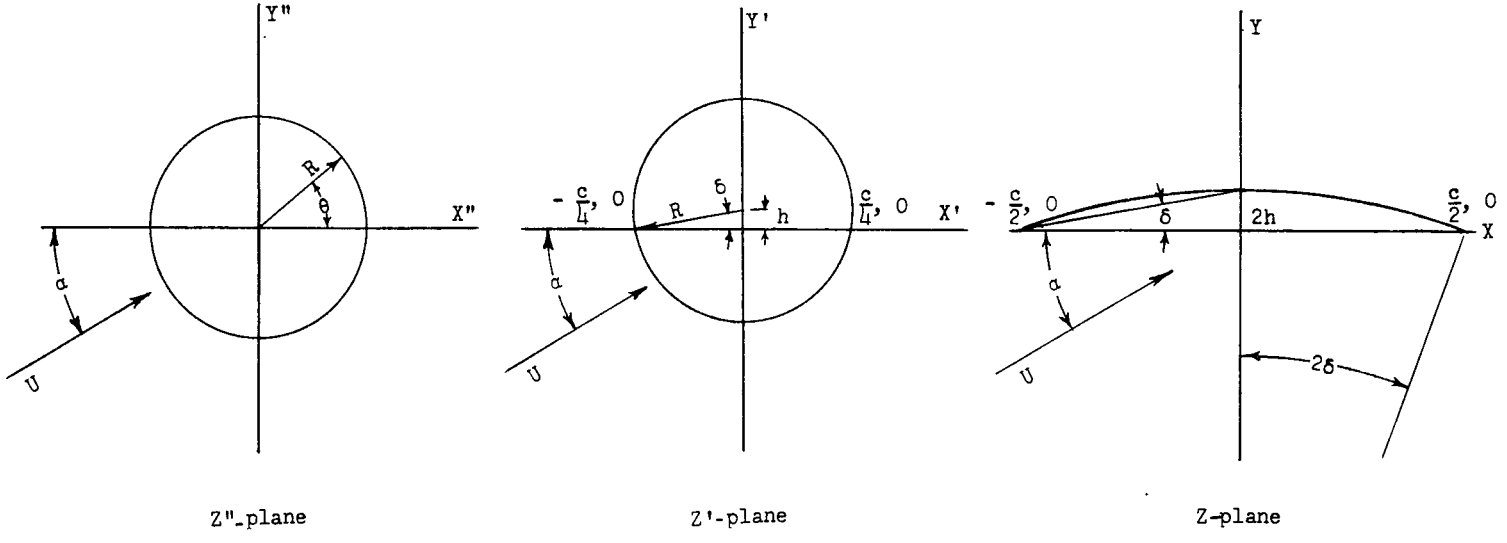

Figure 2.- Conformal transformation of a circle into a circular-arc airfoil.

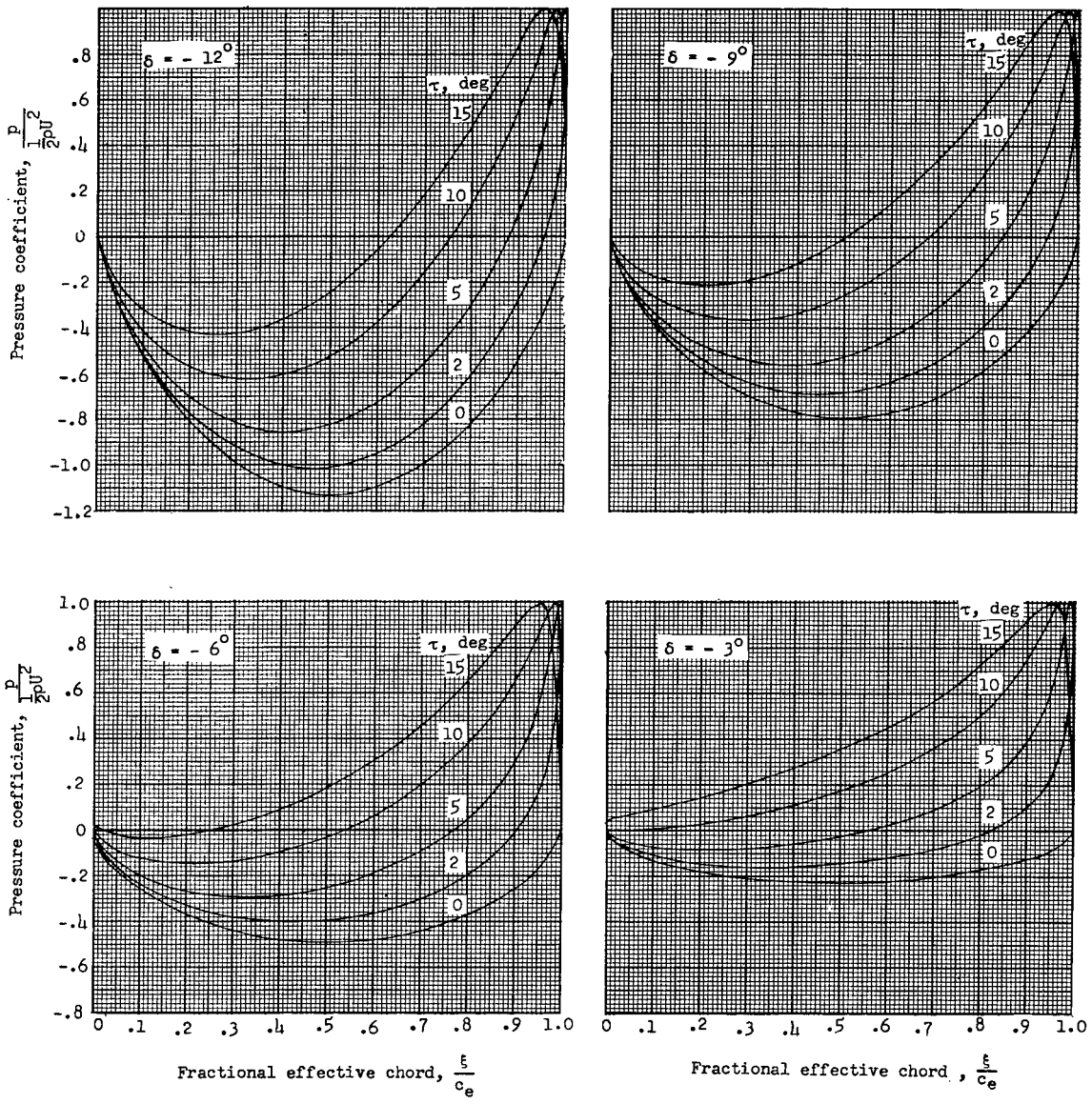

Figure 3.- Variation of lower surface-pressure coefficients with fractional effective chord for two-dimensional cambered plates having a wide range of camber δ.

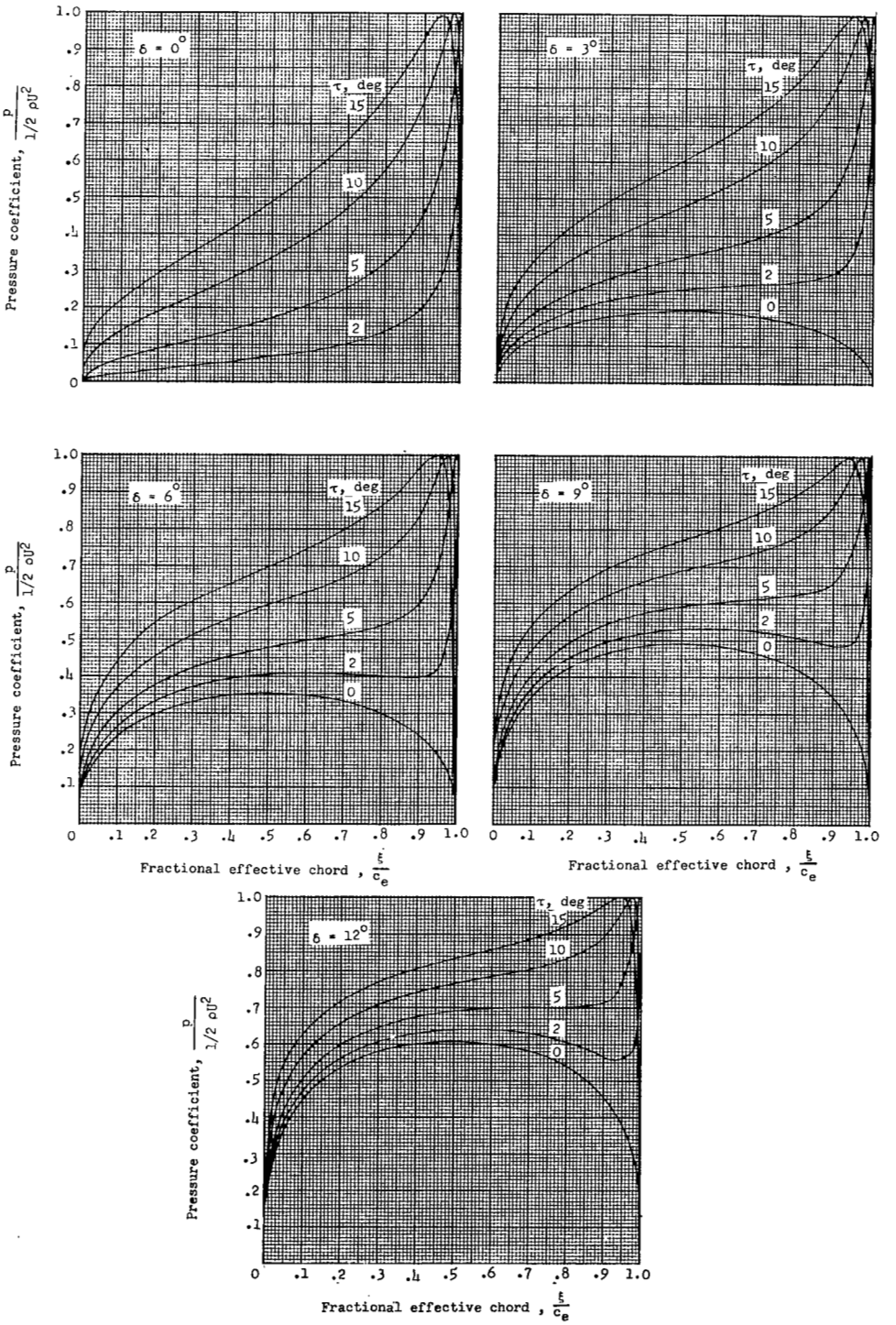

Figure 3.- Concluded.

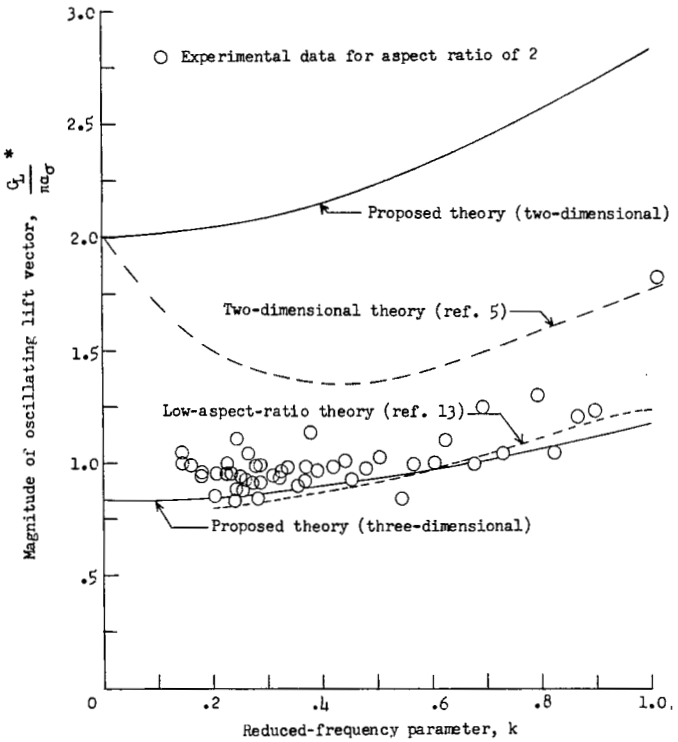

(a) Variation of oscillating lift vector with reduced-frequency parameter.

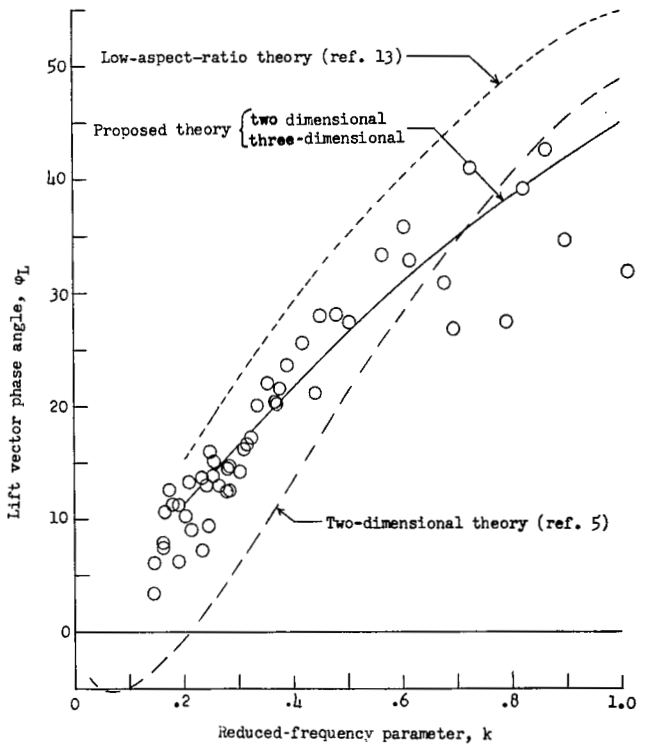

(b) Variation of lift vector phase angle with reduced-frequency parameter.

Figure 4.- Comparison of theoretical and experimental lift vectors and phase angles for an oscillating airfoil immersed in an air stream.

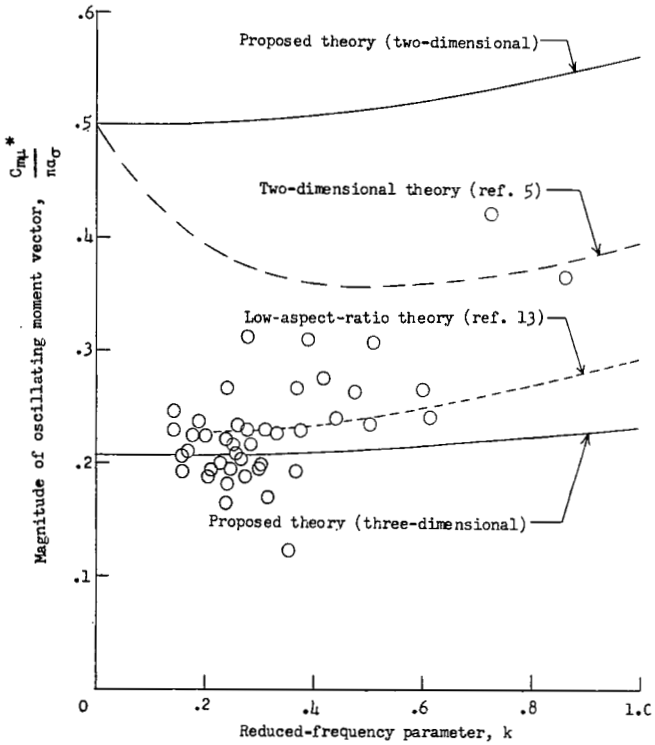

(c) Variation of oscillating moment vector with reduced-frequency parameter.

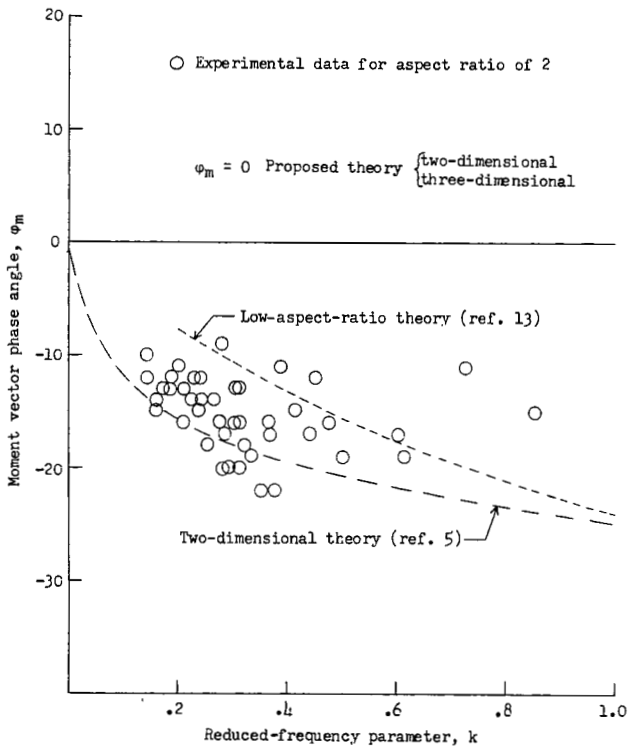

(d) Variation of moment vector phase angle with reduced-frequency parameter.

Figure 4.- Concluded.

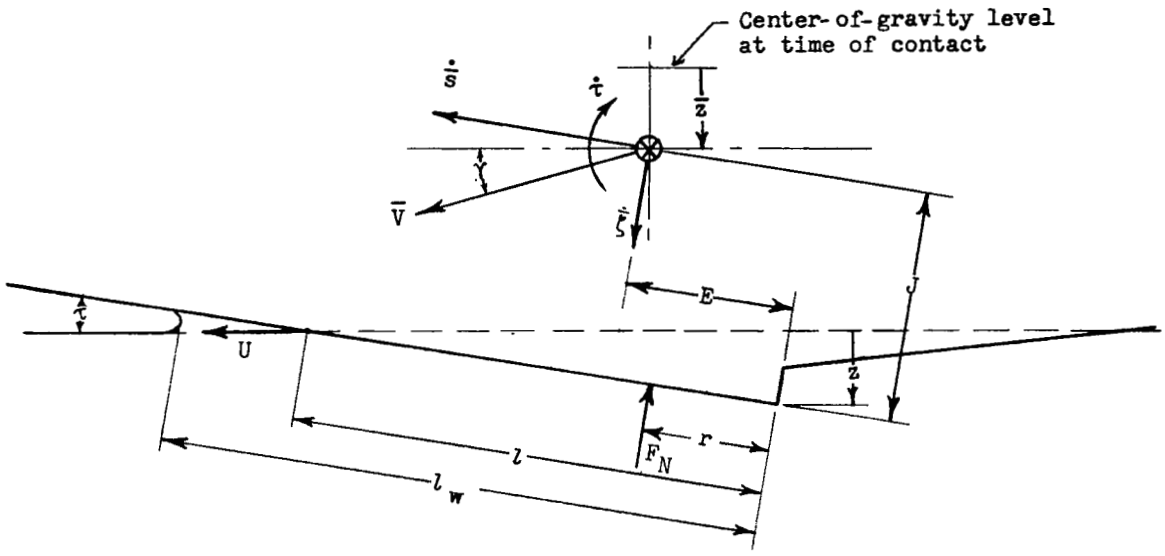

(a) Narrow trimming hull.

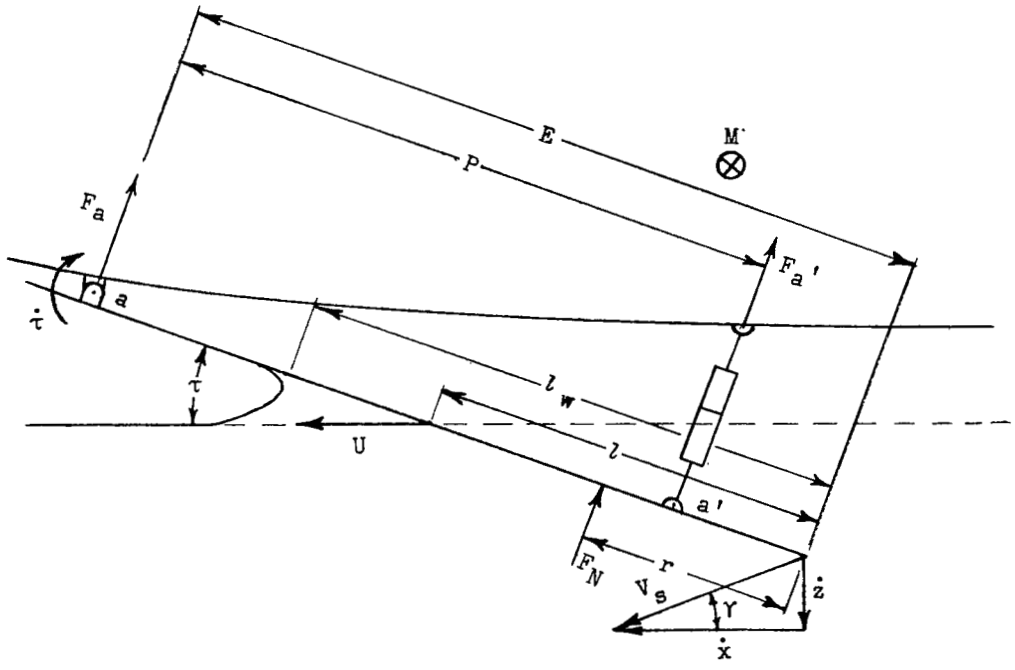

(b) Shock-mounted hydro-skis.

Figure 5.- Geometric relations of trimming bodies during water impact.

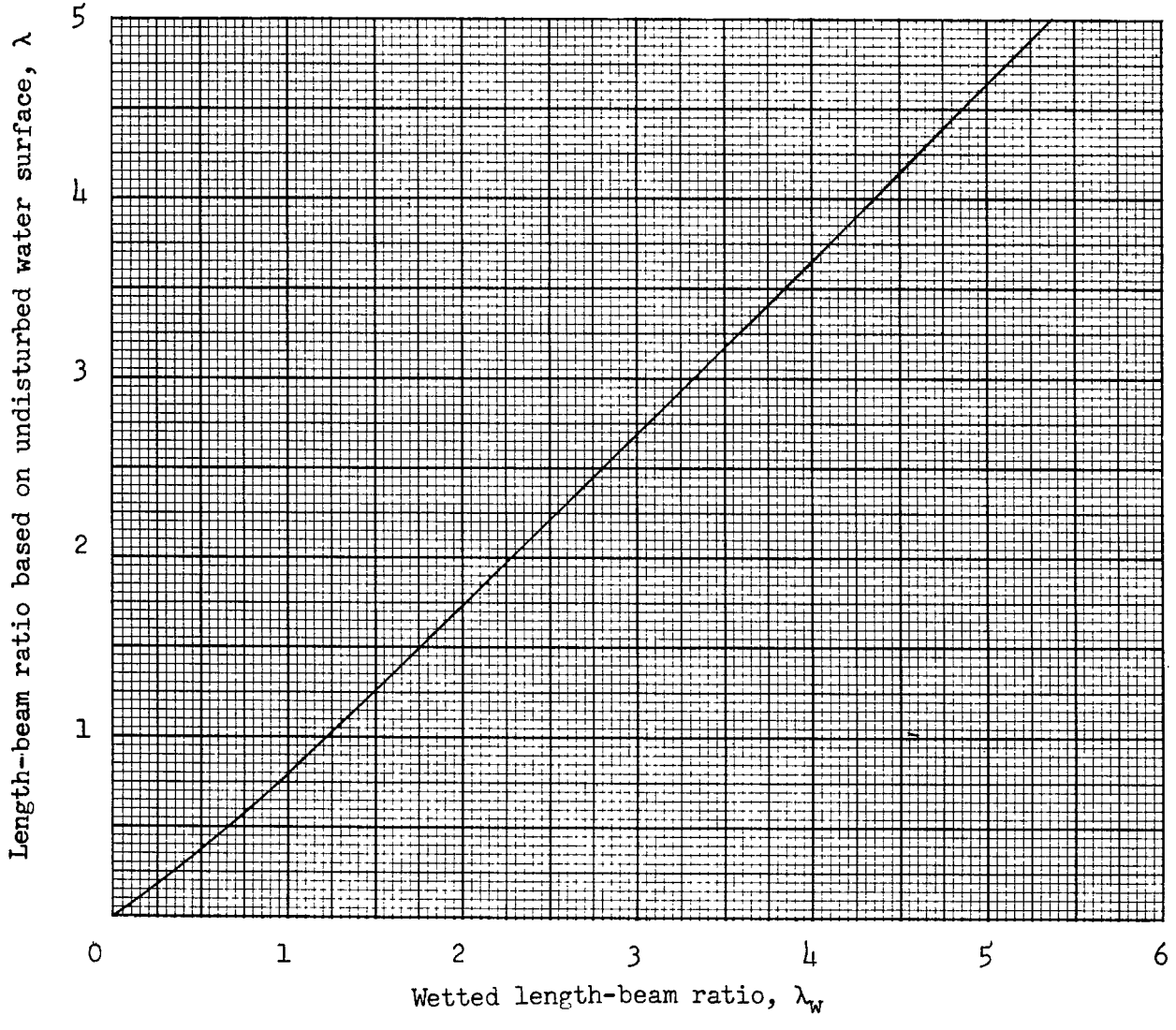

Figure 6.- Variation due to water rise of ratio of wetted length to beam for a flat plate.

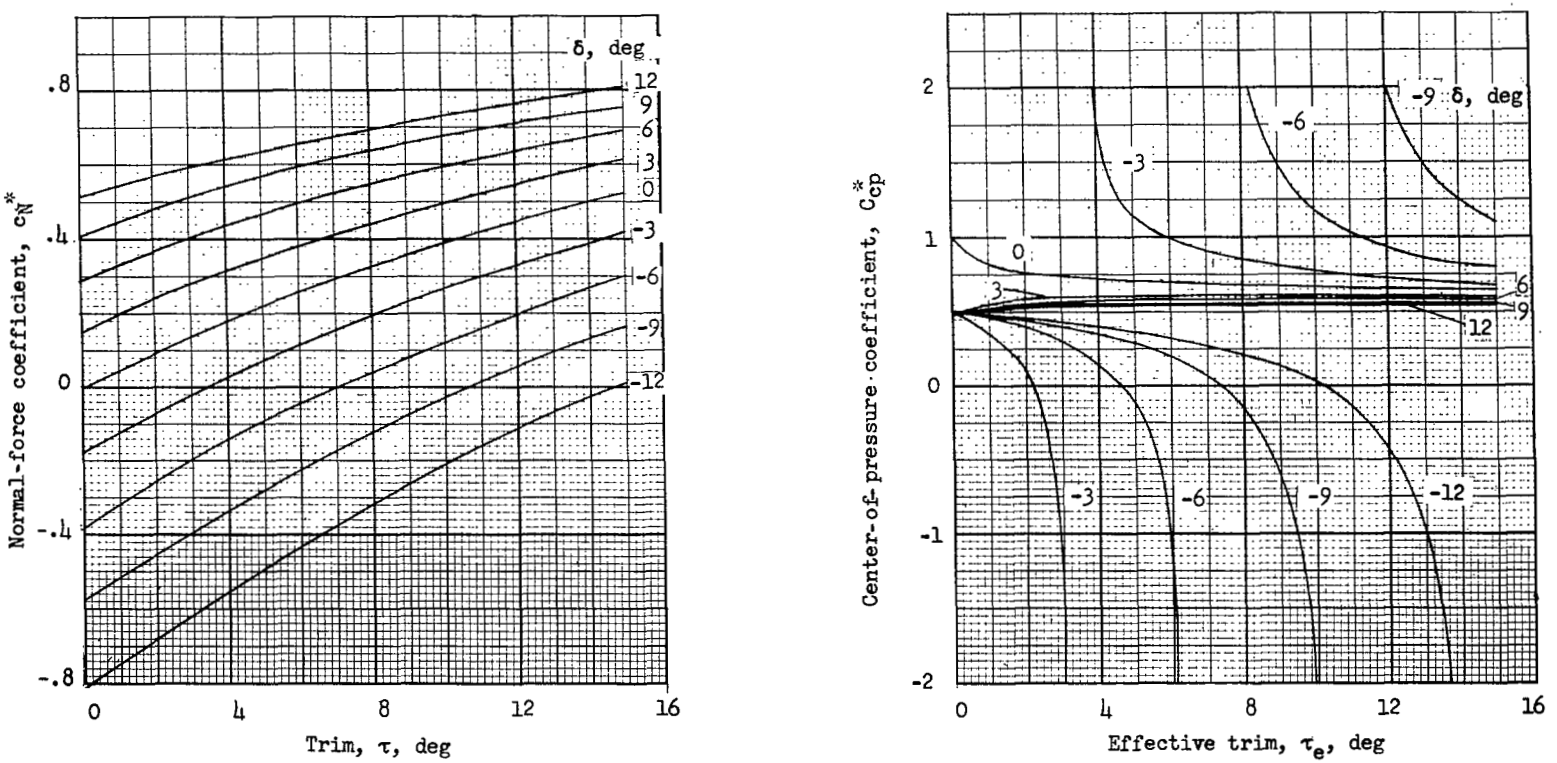

Figure 7.- Variation of two-dimensional normal-force and center-of-pressure coefficients on the lower surface of a cambered plate with trim τ and effective camber δ.

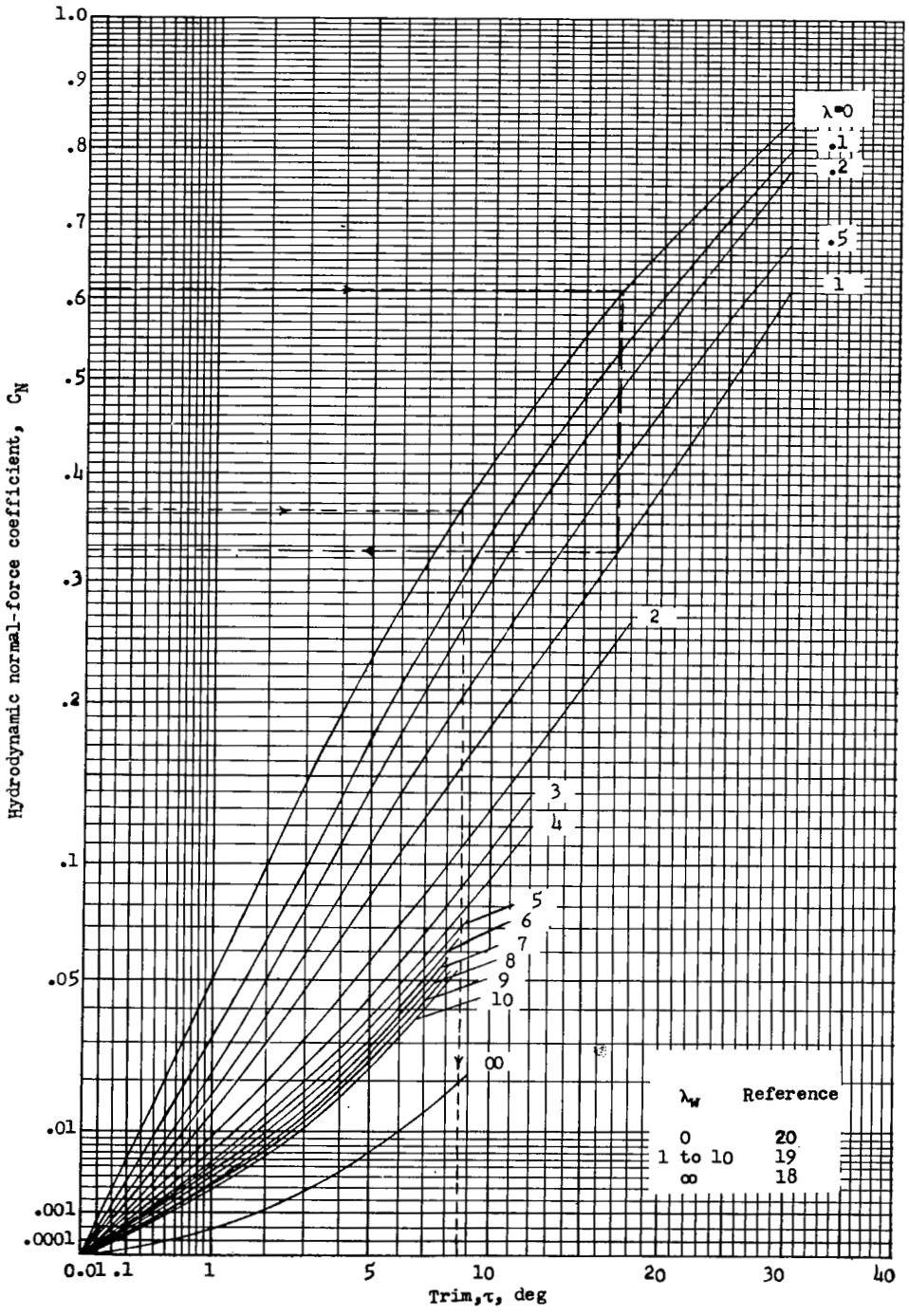

Figure 8.- Variation of planing normal-force coefficient on the level surface of a flat rectangular plate with trim and wetted-length-beam ratio λ_W.

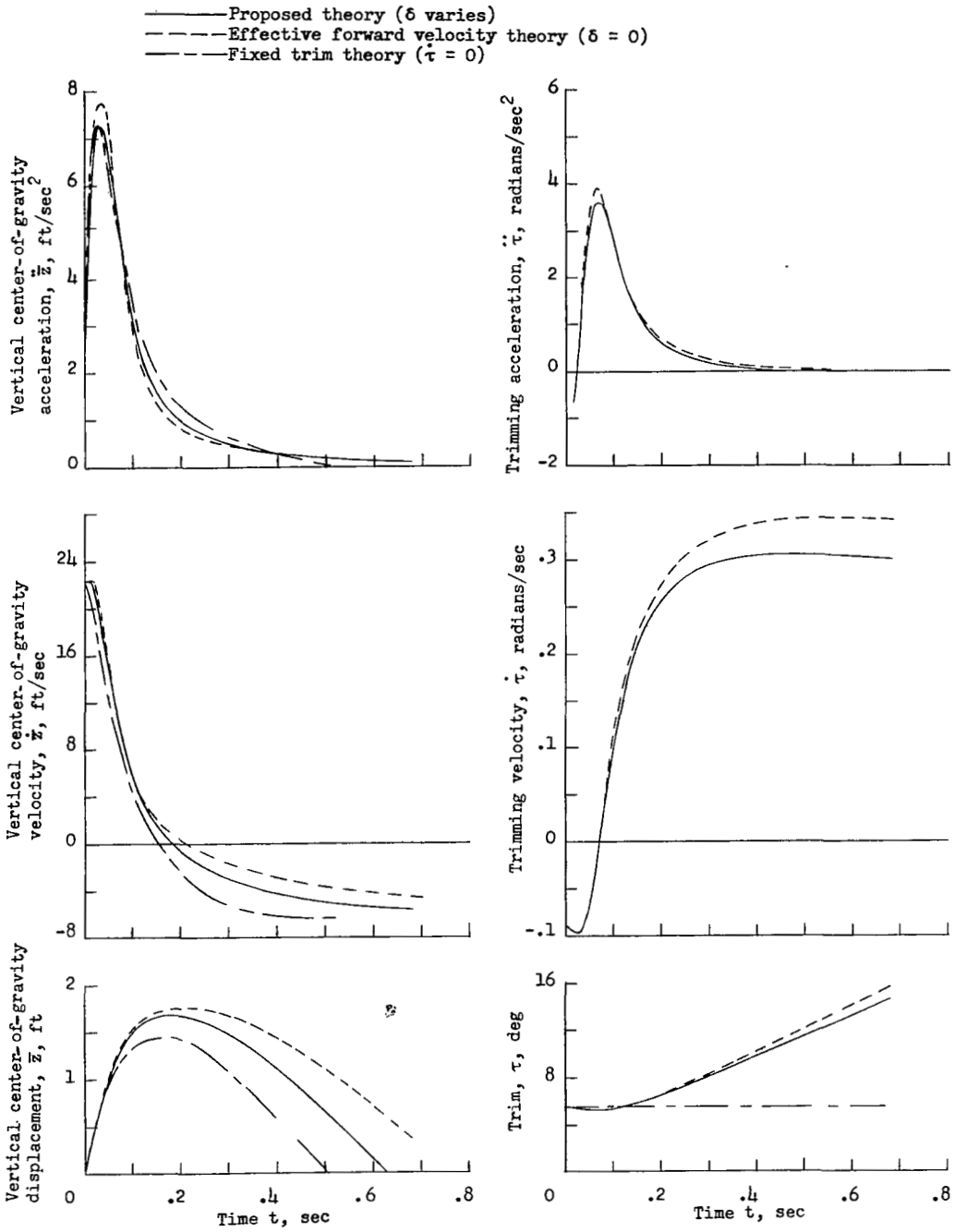

(a) Run I.

Figure 9.- Comparison of approximate theories for computing motion-time histories of freely trimming, narrow flying boats during water impact. For initial conditions see table I.

[redacted]

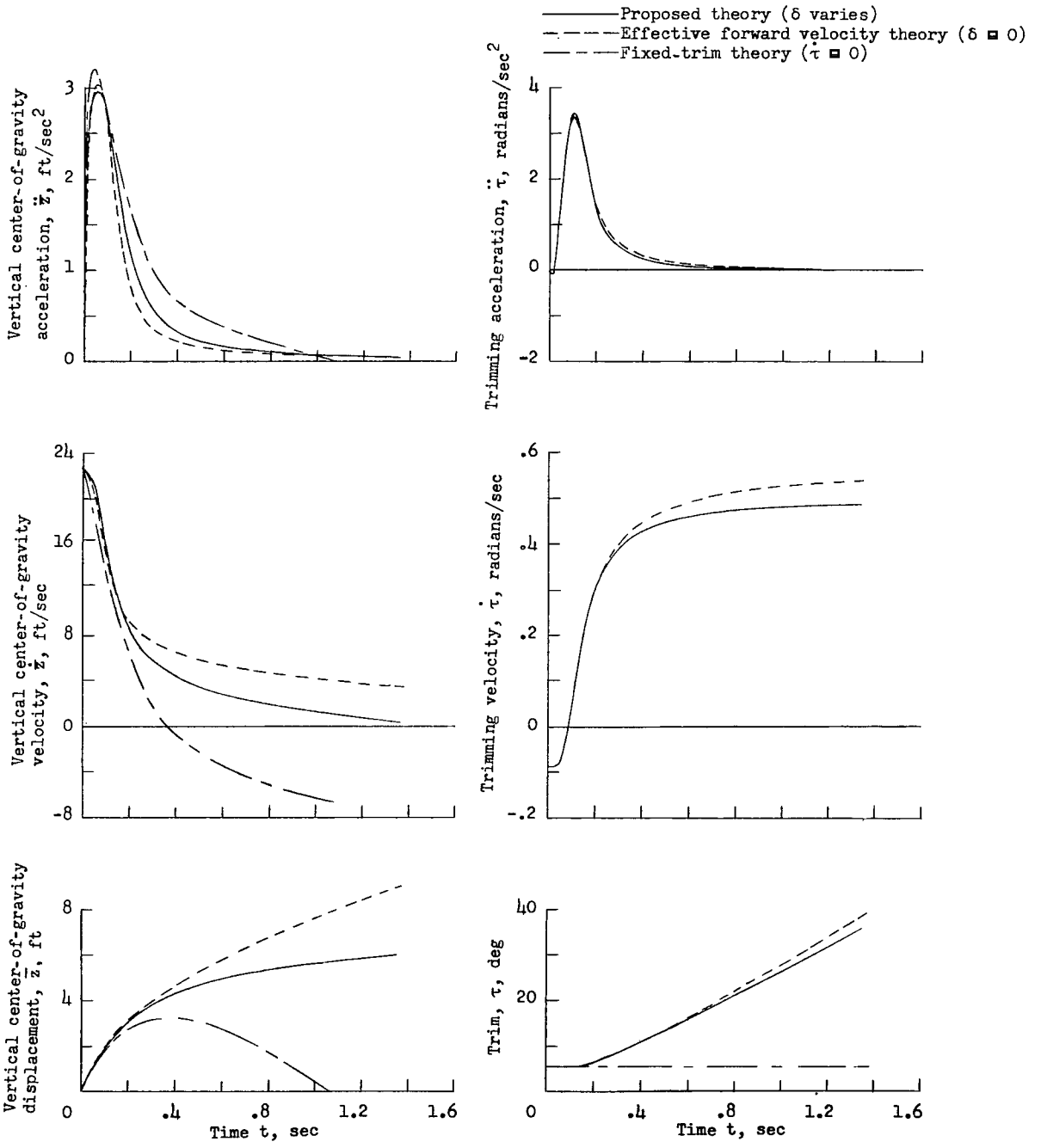

(b) Run II.

Figure 9.- Concluded.

[redacted]

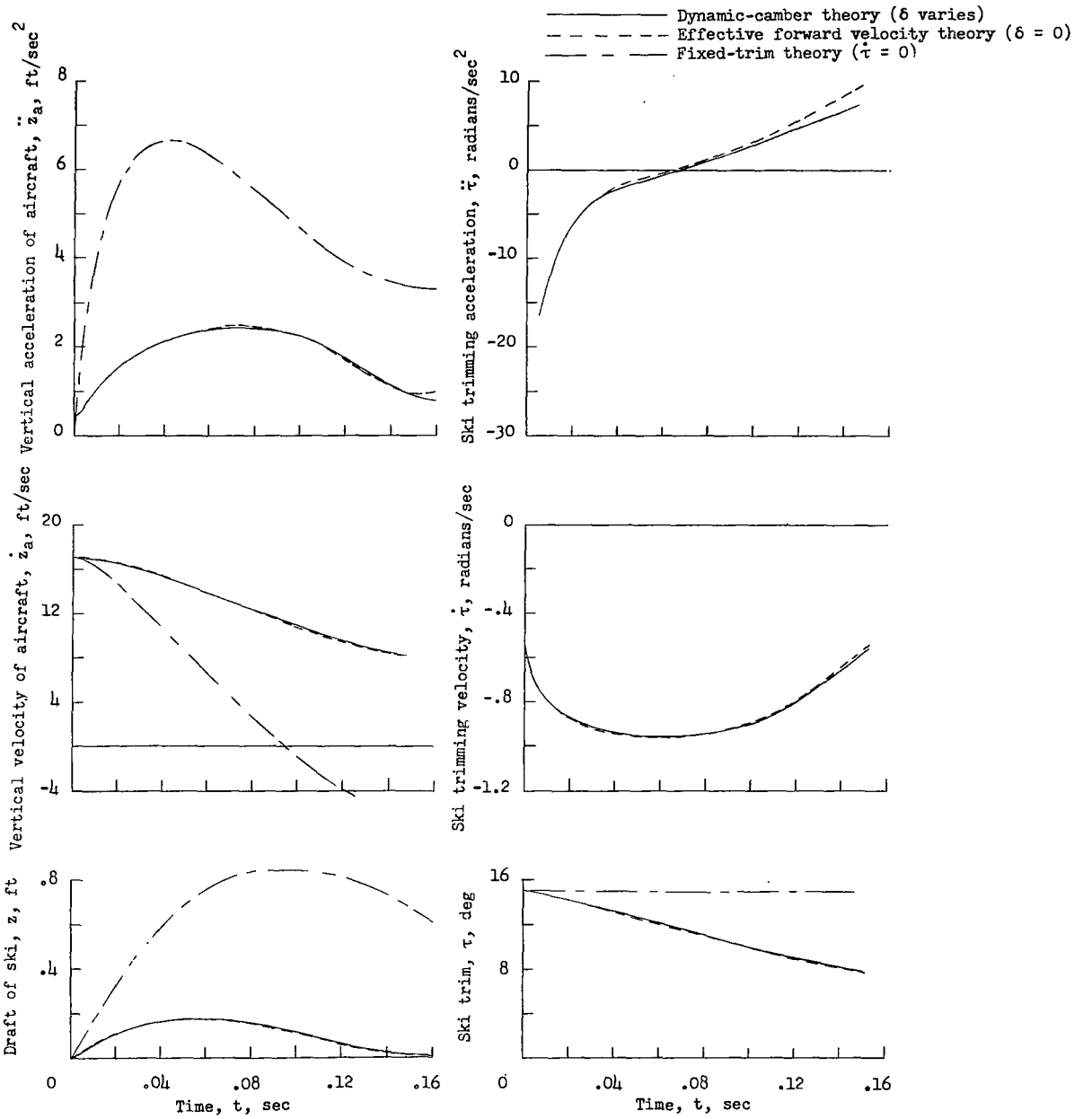

(a) Run III, forward pivot location.

Figure 10.- Comparison of approximate theories for computing motion-time histories during water impacts of aircraft equipped with trimming, shock-strut-mounted hydro-skis. For initial conditions see table I.

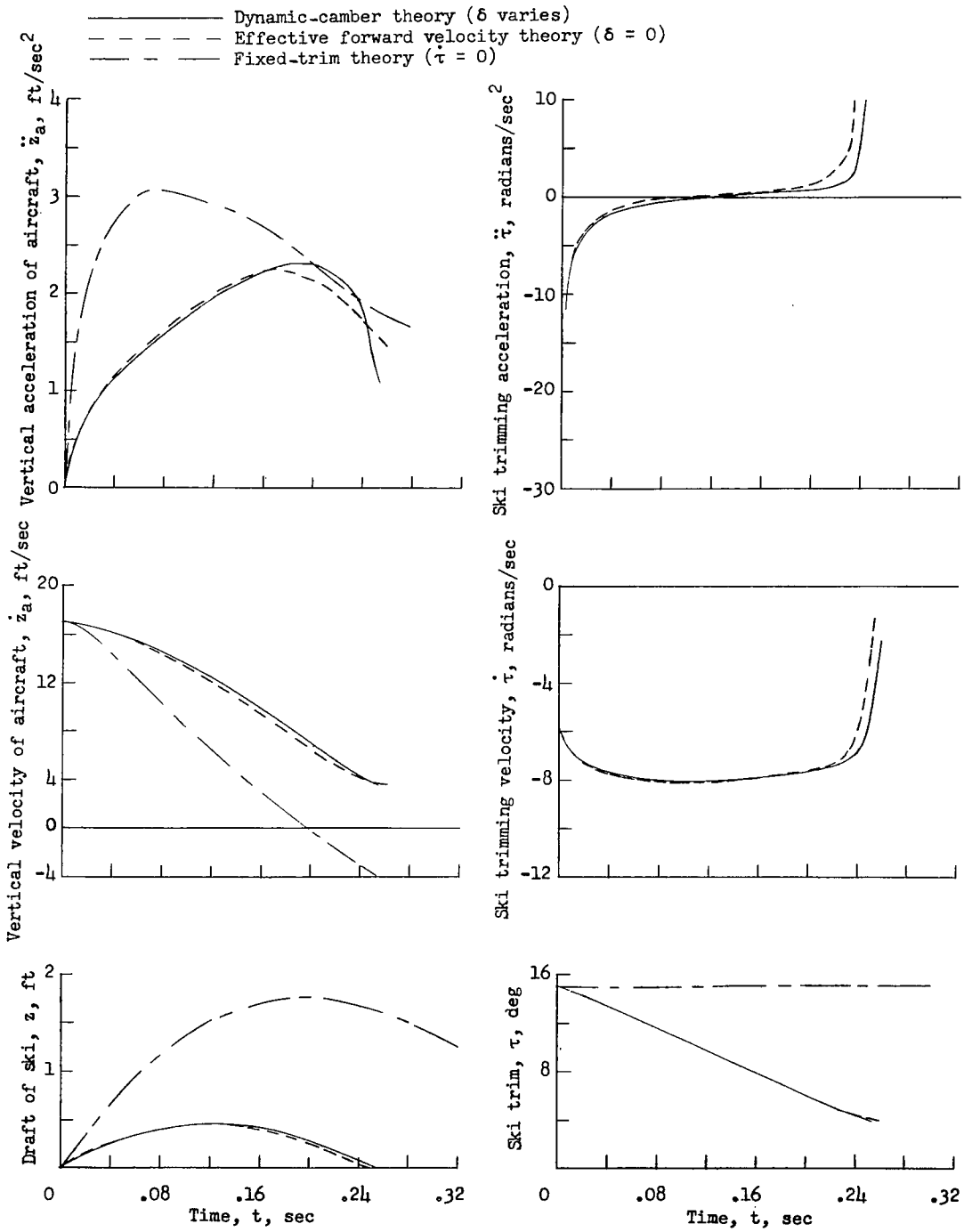

(b) Run IV, forward pivot location.

Figure 10.- Concluded.